PHOTOLUMINESCENCE AND INFRARED ABSORPTION SPECTROSCOPY OF NITROGEN-OXYGEN DONORS IN SILICON

by

Lori Lenchyshyn

B.Sc., University of Waterloo, 1987

THESIS SUBMITTED IN PARTIAL FULFILLMENT OF
THE REQUIREMENTS FOR THE DEGREE OF
MASTER OF SCIENCE
in the Department
of Physics

© Lori Lenchyshyn 1990

SIMON FRASER UNIVERSITY

March 1990

All rights reserved. This work may not be
reproduced in whole or in part, by photocopy
or other means without permission of the author.

APPROVAL

Name: Lori Lenchyshyn

Degree: Master of Science

Title of Thesis: Photoluminescence and Infrared Absorption Spectroscopy of Nitrogen-Oxygen Donors in Silicon

Examining Committee:

Chairman: Dr. K. Colbow

Dr. M.L.W. Thewalt
Senior Supervisor

Dr. E.D. Crozier

Dr. M. Wortis

Dr. J.C. Irwin
Examiner
Physics Department
Simon Fraser University

Date Approved: March 26 1990

PARTIAL COPYRIGHT LICENSE

I hereby grant to Simon Fraser University the right to lend my thesis, project or extended essay (the title of which is shown below) to users of the Simon Fraser University Library, and to make partial or single copies only for such users or in response to a request from the library of any other university, or other educational institution, on its own behalf or for one of its users. I further agree that permission for multiple copying of this work for scholarly purposes may be granted by me or the Dean of Graduate Studies. It is understood that copying or publication of this work for financial gain shall not be allowed without my written permission.

Title of Thesis/~~Project/Extended Essay~~

Photoluminescence and Infrared Absorption Spectroscopy of Nitrogen-Oxygen Donors in Silicon

Author:

(signature)

Lori Lenchyshyn

(name)

April 3 1990

(date)

ABSTRACT

Many interesting and technologically important defects are generated in silicon when impurities such as nitrogen, oxygen and carbon group together and become electrically active complexes. The series of nitrogen-oxygen donors recently observed in infrared absorption spectra of Czochralski silicon has been studied here for the first time using photoluminescence spectroscopy. These complexes are found to bind excitons and multiexcitonic complexes, with an exciton localization energy of 3.9 meV. Conclusive identification of the exciton binding centers with the nitrogen-oxygen donors seen in absorption is provided by the observation of bound exciton two-electron transitions. These transitions leave the donors in their 2s or $2p_{\pm}$ excited states.

Despite the wide use of nitrogen in semiconductor processing, its rate of diffusion in silicon is still a matter of some debate. Recent publications place the diffusion coefficient at 1270°C at about 2×10^{-6} cm^2/sec, conflicting with earlier values by five orders of magnitude. The diffusion profile is determined here using the photoluminescence intensity of the nitrogen-oxygen donors. A diffusion coefficient of $1.3 \pm 0.8 \times 10^{-6}$ cm^2/sec is obtained, in agreement with the recent findings.

ACKNOWLEDGEMENT

I would like to thank my senior supervisor, Dr. M.L.W. Thewalt, for sharing his insight and experimental skills during the course of this project. Special thanks to Dr. A.G. Steele, and all the members of the Thewalt lab for their help and encouragement.

Financial support from the Natural Sciences and Engineering Research Council of Canada, Simon Fraser University, and Dr. M.L.W. Thewalt was greatly appreciated.

TABLE OF CONTENTS

Approval ii

Abstract iii

Acknowledgement iv

List of Tables vii

List of Figures viii

List of Abbreviations ix

Chapter 1 Optical Characterization of Impurities in Silicon

1.1 Introduction 1

1.2 Effective Mass Theory 2

1.3 Infrared Absorption Spectroscopy 5

1.4 Bound Excitons and Bound Multiexciton Complexes...... 6

1.5 Photoluminescence Spectroscopy 9

Chapter 2 Experimental Techniques

2.1 Fourier Transform Infrared Absorption Spectroscopy .. 14

2.2 Photoluminescence Spectroscopy 16

2.3 Sample Preparation 19

Chapter 3 Nitrogen-Oxygen Donors in Silicon

3.1 Introduction 21

3.2 Infrared Absorption Results 24

3.3 Photoluminescence Results 30

3.4 Conclusion 38

TABLE OF CONTENTS (CONTINUED)

Chapter 4 Nitrogen Diffusion in Silicon

4.1 Introduction 40

4.2 Diffusion Coefficient Determined by Photoluminescence 44

4.3 Conclusion 53

References 56

LIST OF TABLES

3.1 N-O Donor IR Absorption Lines 27

3.2 N-O Donor Ionization Energies 28

3.3 N-O Donor Photoluminescence Lines 37

4.1 Diffusion Coefficient of Nitrogen in Silicon 42

LIST OF FIGURES

2.1 IR Absorption Experimental Setup 15

2.2 Photoluminescence Experimental Setup 17

3.1 N-O Donor IR Absorption Spectrum 26

3.2 N-O Donor PL Spectrum 31

3.3 N-O Donor BMEC Intensity vs Excitation Power 33

3.4 N-O Donor Two-electron PL Spectrum 35

4.1 Depth Study Geometry 45

4.2 N-O Donor PL Spectra vs Depth 46

4.3 N-O Donor BMEC Integrated Intensity vs Depth 49

4.4 Best Fit for Constant Surface Concentration Diffusion Source ... 52

4.5 Profiles for Limited Diffusion Source 54

LIST OF ABBREVIATIONS

BE	bound exciton
BMEC	bound multiexcitonic complex
Cz	Czochralski
EHD	electron-hole droplet
EMT	effective mass theory
FE	free exciton
FWHM	full width half maximum
FZ	float zone
IR	infrared
LO	longitudinal optical (phonon)
NP	no-phonon
PL	photoluminescence
STD	shallow thermal donor
TA	transverse acoustic (phonon)
TO	transverse optical (phonon)

CHAPTER 1 OPTICAL CHARACTERIZATION OF IMPURITIES IN SILICON

1.1 Introduction

As device production pushes for ever increasing purity in semiconductor materials, there is also a demand for identifying impurities and their properties. Optical techniques have been developed that detect various impurity related electronic or vibrational transitions. This thesis describes the application of photoluminescence (PL) spectroscopy and infrared (IR) absorption spectroscopy to determine the electronic structure and growth characteristics of nitrogen-oxygen donors in Si. A detailed account of these techniques is given later in this chapter. Several review articles [87H, 81R] describe the use of these, and other optical methods, in characterizing semiconductor materials, including photothermal ionization spectroscopy (PTIS), local vibrational mode spectroscopy, Raman spectroscopy and photoconductivity.

Preceding the sections covering IR absorption spectroscopy (Section 1.3),and PL spectroscopy (Section 1.5), is a description of the electronic levels relevant to each technique. In IR absorption the valence electron (or hole) of a neutral impurity is promoted from its ground state to an excited state. These energy levels are to a first approximation given by the hydrogenic scheme of effective mass theory (EMT). The following section reviews EMT for impurities in Si. In photoluminescence, a photon of characteristic energy is emitted when an exciton bound to an impurity recombines. Section 1.4 describes bound excitons and bound multiexciton complexes.

1.2 Effective Mass Theory

Effective mass theory describes the electronic energy levels of the valence electron (or hole) of an impurity atom contained in the crystal lattice. Treating the ionized impurity core and its valence electron (or hole) as analogous to the hydrogen atom, energy levels relative to that of the free particle (ie. an electron in the conduction band or hole in the valence band) are:

$$E_n = \frac{-m^* e^4}{2h^2 \varepsilon^2 n^2} \qquad (n=1,2,3,\ldots) \qquad (1.1)$$

where m^* is the electron (or hole) effective mass (which in reality need not be isotropic), and ε is the dielectric constant of the host lattice. The factor ε accounts for dielectric screening of the Coulomb attraction compared to that for the atom in free space. Similarly, the effective mass must be used since the electron (or hole) interacts with the crystal lattice such that it behaves as if it has mass m^*, often much less than that of an electron in free space. Substituting appropriate values for m^* and ε in Si gives a Bohr radius of about 100 Å, and therefore the use of a macroscopic dielectric constant is consistent. Typical impurity ionization energies are in the meV range, compared to being of the order of eV for the atom in free space.

This simple presentation of EMT energy levels can be justified more rigorously by solving the Schrodinger equation with a potential term $U(r) \cong \pm e^2/\varepsilon r$, due to the presence of the impurity ion in an otherwise perfect crystal. This can be treated in a number of ways, as reviewed by Bassani and Pastor Parravicini [75B], Lannoo and Bourgoin [81L], and

Ramdas and Rodriguez [81R]. Following the approach given in the classic paper of Kohn and Luttinger [55K]), the bound valence electron (or hole) wave function, $\Phi(\mathbf{r})$, is written as an expansion in terms of the Bloch functions, $\psi(\mathbf{k},\mathbf{r})$, of the unperturbed crystal:

$$\Phi(\mathbf{r}) = \int d\mathbf{k}\ \phi(\mathbf{k})\ \psi(\mathbf{k},\mathbf{r}) \tag{1.2}$$

where $\phi(\mathbf{k})$ is the Fourier transform of an envelope function $\phi(\mathbf{r})$. The effective mass Hamiltonian for $\phi(\mathbf{r})$ can can then be shown to take the form:

$$H = \frac{\hbar^2}{2}\left[\frac{1}{m_x^*}\frac{\partial^2}{\partial x^2} + \frac{1}{m_y^*}\frac{\partial^2}{\partial y^2} + \frac{1}{m_z^*}\frac{\partial^2}{\partial z^2}\right] \pm \frac{e^2}{\epsilon r} \tag{1.3}$$

where the effective masses along the three axes m_x^*, m_y^*, and m_z^* are the values at the band extrema. For an isotropic system $m_x^* = m_y^* = m_z^* = m^*$, so that the problem reduces to solutions of the hydrogenic Schrodinger equation, as above.

For acceptors in Si, the solutions to the effective mass Hamiltonian are complicated by the fact that the valence band maximum in Si is degenerate. Theoretical discussions are given in a number of papers, including Onton *et al.* [67O], and Baldereschi and Lipari [74B], but they are not relevant here since this thesis focuses on a donor-like complex.

The situation for donors in Si is also more complicated than that of the isotropic system discussed above. There are six equivalent conduction band minima located 85% of the way to the zone boundary in the <100> directions. The constant energy surfaces in k-space, about each of the minima, are ellipses of revolution. The effective mass is

therefore anisotropic, with values perpendicular and parallel to each ellipse principal axis being $m_l^* \cong 0.98m_o$ and $m_t^* \cong 0.19m_o$, where m_o is the free space electron mass [81S]. As discussed below, this band structure results in valley-orbit splitting of the ground state as a consequence of the six equivalent band minima, and splitting of excited states due to the anisotropy of the effective mass.

Valley-orbit splitting can be understood by constructing wave functions which conform to the local symmetry of the impurity [55K, 75B, 81L, 81R]. Since the conduction band is identical at each of the six minima, the donor states are expected to be six-fold degenerate, not counting spin. It is this degeneracy that is split because of the different chemical potential of the impurity. In the vicinity of a substitutional impurity the local symmetry is lowered from the O_h point group of the pure Si lattice to the tetrahedral point group T_d. The resulting wave functions can be shown to be basis functions for the irreducible representations A_1+E+T_2 in the T_d point group. Therefore the donor ground state is valley-orbit split into a singlet 1s(A_1), a doublet 1s(E) and a triplet 1s(T_2). In Si, the 1s(A_1) state is typically the lowest in energy. Electrons in excited states have a low probability of coming close to the impurity site, particularly for odd parity states, so that valley orbit splitting can be neglected.

For excited states the effective mass Hamiltonian with the appropriate values for m^* is solved using perturbative methods. For states with orbital quantum number, l, greater than 1, the anisotropy of m^* results in level splitting for the different values of azimuthal quantum number m_l ($-l < m_l < l$). Thus a p-state is split into a singlet p_o, with m=0, and a doublet $p_{\pm}$, with m=±1, similarly a d-state becomes

d_o, $d_{\pm1}$, $d_{\pm2}$, and so on. Energy separations between the donor excited states were originally calculated by Faulkner, and agreed quite well with experimental observations (within 0.05 meV for phosphorus) [69F].

The theoretical ground state energies are not in as close agreement with experimental data, since for these states the nature of the specific donor core becomes important. This applies especially for the A_1 state which has the largest amplitude at the donor site. This shift in ground state ionization energy is known as the central cell correction, but is not well understood theoretically. The spectra for different impurities therefore show similar excited state energy level separations, but are shifted in energy depending on the location of the ground state ($1s(A_1)$) relative to the impurity ionization energy.

1.3 Infrared Absorption Spectroscopy

By absorbing a photon the impurity valence electron (or hole) can make an electronic dipole transition to an excited state. Transitions from the ground to excited states are in the meV range, corresponding to absorption of radiation in the mid to far infrared region. Experiments must be conducted at cryogenic temperatures to prevent ionization of impurities and thermally broadened linewidths. Since high excited states are not influenced strongly by the nature of the impurity, the temperature is usually kept low enough that initially only the ground state is populated. This corresponds to about 10 K for shallow impurities in Si.

Selection rules for atoms in free space allow electronic dipole transitions only between states of opposite parity. Considering only one conduction band valley, the same rules apply for donors in Si. However, since the ground state is valley-orbit split, so-called EMT forbidden transitions can become what is known as symmetry allowed. This applies for example to the transition between the $1s(A_1)$ and $1s(T_2)$ state, which are of even and odd parity respectively. IR absorption provides experimental values of energy separations for odd parity excited states, and valley-orbit splitting of the ground state. Such data was summarized by Faulkner [69F] for typical shallow donors in Si, including Li, P, As, Sb, and Bi, and compared favourably with his EMT estimates.

1.4 Bound Excitons and Bound Multiexciton Complexes

Semiconductor impurities have been shown to be capable of binding an electron-hole pair in a stable complex referred to as a bound exciton (BE). The existence of these states was predicted in 1958 by Lampert [58L], using the analogy of particles described by EMT to those found in hydrogenic systems. Several years later Haynes observed BEs experimentally [60H]. This section covers the theoretical understanding of BEs, while the next deals with their observation through PL spectroscopy.

The BE can be thought of as a free exciton (FE) which lowers its energy by binding to an impurity. In covalent materials, such as

semiconductors, the FE is described in the Wannier-Mott limit. In this model the electron and hole wave functions extend over many atomic separations, so that the Coulomb attraction between them is simply described by hydrogenic energy levels:

$$E_n = \frac{-\mu e^4}{2\hbar^2 \varepsilon^2 n^2} \qquad (n=1,2,3,\ldots) \qquad (1.4)$$

where μ is the exciton reduced mass, $\mu = 1/(m_e^{-1} + m_h^{-1})$, and E_n is relative to the band edge. Since the impurity ion core and its valence electron (or hole) are also described by hydrogenic levels, the binding of the exciton to the neutral impurity is analogous to the formation of a hydrogen molecule.

Unlike FEs, which can move through the crystal, the BE is localized at the impurity. Therefore the total energy of the BE does not include a kinetic energy term. Broadening of the energy spectrum due to the Maxwell-Boltzmann distribution in kinetic energies, which is typical of the FE, is absent for BEs. The energy difference between the BE and a zero kinetic energy FE is known as the BE binding energy (E_{BX}). It is the binding energy that is of interest in characterizing Si, since it is usually unique to a particular impurity.

Differences in binding energy for different impurities are a consequence of the local potential and strain field arising from the presence of the impurity ion core. These effects are usually treated as a perturbation to effective mass theory known as the central cell correction. Introducing the central cell potential, V_c, the BE binding energy and neutral impurity ionization energy become:

$$E_{BX} = (E_{BX})_{EMT} + V_c \, \delta\rho_c \tag{1.5a}$$

$$E_i = (E_i)_{EMT} + V_c \, \rho_c \tag{1.5b}$$

where ρ_c is the charge in the impurity central cell and $\delta\rho_c$ is the additional charge due to the BE. The equations are combined to give [73D, 76B]:

$$E_{BX} = \left[(E_{BX})_{EMT} - (E_i)_{EMT} \frac{\delta\rho_c}{\rho_c} \right] + \frac{\delta\rho_c}{\rho_c} E_i \tag{1.6}$$

This relationship between exciton binding energy and impurity ionization energy is used to explain the empirical relation known as Haynes' rule [60H]:

$$E_{BX} = a \, E_i + b \tag{1.7}$$

Haynes' rule is obeyed to some extent in most semiconductors [79D], but with constants a and b varying among different materials. In Si a is approximately 0.1, while b is about zero [60H].

It is also possible for more than one exciton to bind to an impurity forming what is known as a bound multiexciton complex (BMEC) [82T]. The existence of these complexes was the subject of much debate, the original BMEC concept having been proposed by Kaminskii and Pokrovskii [70K] , seven years before its acceptance in light of the Kirczenow shell model [77Ka]. Overwhelming experimental support for the shell model in photoluminescence studies of BMEC behaviour under magnetic fields and uniaxial stress [76D, 77Ha, 77Ta, 78Tb], finally eliminated the last remaining opposing model, which involved a BE-polyexciton complex [76M].

In the shell model, the electrons and holes which make up the BMEC

fill degenerate single particle levels in shells. The shells are determined by taking into account the symmetry of the impurity, tetrahedral for most impurities in Si, and the effects of the semiconductor band structure. This gives a lowest hole shell with the four-fold degeneracy of the valence band edge, labelled Γ_8. The twelve-fold degeneracy of the conduction band minima is lifted by valley-orbit splitting to give levels Γ_1, Γ_3 and Γ_5 (or equivalently A_1, E, and T_2 in the notation of Section 1.2) with degeneracies 2, 4, and 6 respectively. The Γ_3 to Γ_5 splitting is assumed negligible except for the isolated neutral donor.

For Si this model has been shown to explain the number of levels seen in unperturbed spectra, Zeeman spectroscopy, uniaxial stress , as well as trends in transition intensities [82T]. The shell model does not encompass theoretical calculations of BMEC binding energies. Because BMECs make up a many-particle system in which correlation between particles is significant, this is a difficult problem which has yet to be solved [82T].

1.5 Photoluminescence Spectroscopy

Photoluminescence is the radiation emitted following excitation to a nonequilibrium state by absorption of energy in the form of light. In a semiconductor, above band gap excitation creates electron-hole pairs, which quickly thermalise to the band edges by emitting phonons. At low temperatures these electrons and holes can then bind together to form

FEs, or in the presence of impurities, BEs. Lifetimes of excitons in Si range from milliseconds to nanoseconds [86Sb], after which the exciton electron and hole recombine, sometimes emitting a characteristic photon observed as the principal BE ($\hbar\omega_{BE}$) or FE ($\hbar\omega_{FE}$) line in PL.

In indirect semiconductors electron-hole recombination must in general be accompanied by emission of a momentum conserving phonon. The emitted photon is therefore shifted down in energy by the amount required for phonon creation ($\hbar\omega_{ph}$):

$$\hbar\omega_{FE} = E_g - E_{FE} - \hbar\omega_{ph} \quad (1.8a)$$

$$\hbar\omega_{BE} = E_g - E_{FE} - E_{BX} - \hbar\omega_{ph} \quad (1.8b)$$

where $\hbar\omega_{FE}$ refers to an FE with zero kinetic energy, E_g is the host band gap, E_{FE} is the energy binding the e-h pair, and E_{BX} is the exciton binding energy. The PL spectrum consists of a number of phonon replicas, with the TO most intense for FEs in Si. The LO and TA phonon replicas are also seen, but with reduced intensity. Selection rules for allowed phonon assisted transitions can be derived by considering the symmetry of the phonon involved [75B, 71L]. Momentum conservation for BE recombination can also take place by coupling of the exciton with the impurity, so that for BEs a no-phonon process is sometimes observed [67D].

Although Haynes' rule is often useful, it is difficult to identify unambiguously BE transitions observed in PL with specific donors or acceptors seen in IR absorption. Fortunately a signature of the donor and acceptor excited states is observed in the so-called two electron (2 *e*) and two hole (2 *h*) transitions respectively of the BE [67D]. In this process, when the BE recombines the neutral donor or acceptor is

left in an excited state. The emitted photon is shifted down in energy from the principal BE transition by the impurity ground state to excited state energy difference. Such transitions are very useful when the presence of different impurities with similar values of E_{BX} is obscured by phonon broadening of the principal BE line.

In contrast to the dipole transitions observed in IR absorption, no parity change takes place in 2 *e* or 2 *h* transitions [67D, 76S, 80M]. This is expected since the electric moment is already changed by the electron-hole recombination. The wavefunctions of each particle in the BE consist of a superposition of the ground state (1s) and excited states of the same parity (ns, nd, etc.). After BE recombination, the valence electron (or hole) can be left in one of these excited states. Since 2 *e* and 2 *h* transitions probe the even parity excited states of impurities, this technique provides information complementary to that obtained in IR absorption.

BMECs are observed in PL when one of the excitons belonging to the complex recombines. In fact, to date PL is the only technique available to study BMECs, since their very small oscillator strengths make absorption or excitation spectroscopy impossible [82T]. The BMEC PL features usually appear at energies slightly lower than that for the principal BE of the same impurity. As discussed in the previous section, a satisfactory theoretical model for BMEC binding energies has not yet been found.

The probability of forming a BMEC is expected to increase with a larger density of available FE. Since FE formation can be increased using high excitation energies or very low sample temperatures, BMEC PL is also favoured under these conditions. Experimentally, superlinear

rather than linear excitation power dependence of the PL line intensity distinguishes BMECs from principal BE PL [82T]. Unfortunately the BMEC intensity cannot be increased indefinitely since at very high densities the FE instead condense as electron-hole droplets (EHDs). A thorough description of the EHD can be found in several reviews [77Hb, 77R], but in simple terms it can be described as a degenerate liquid composed of many electrons and holes.

Different relative BMEC intensities for different numbers of bound excitons are also a consequence of the shell model [82T]. Stability of complexes with closed outer electron or hole shells might be expected to reduce the cross-section for FE capture. A very weak PL line is then found for complexes at the start of the next shell. For donor BMECs in Si these drops in intensity are observed after the closing of the first electron shell (the doubly degenerate Γ_1), with the BE, and the first hole shell (the four-fold degenerate Γ_8), with the four exciton BMEC.

In donor BMECs, a large electron wave function amplitude near the impurity site is used to predict the possibility of a strong no-phonon transition. Although the hole is repelled by the positively charged ion core, electrons in the Γ_1 electron state have high probability of being near the donor site and a no-phonon process is seen. Recombination with electrons in the $\Gamma_{3,5}$ state are more likely to involve momentum conserving phonons since their wave function vanishes in the region of the donor. For acceptor BMEC, the electrons are repelled by the negative ion core and therefore effects due to the different wavefunctions for valley-orbit split states are not relevant.

Although it was traditionally used only to identify impurities, recently several authors [78Ta,82K, 87M] have applied PL in determining

absolute impurity concentrations. McL Colley and Lightowlers [87M] published calibrations based on ratios of the BE to FE line intensity for B, P, and Al concentrations from 10^{12} to 10^{15} cm^{-3} in Si. This technique will prove especially fruitful if the calibrations can be extended to very low impurity concentrations ($\leq 10^{11}$ cm^{-3}), where PL has much improved sensitivity over other methods (DLTS, SIMS, resistivity, etc).

CHAPTER 2 EXPERIMENTAL TECHNIQUES

2.1 Fourier Transform Infrared Absorption Spectroscopy

Infrared absorption measurements were taken using a Bruker IFS 113v Fourier transform interferometer. This system is essentially a Michelson interferometer but with the beam directed using a two-sided moving mirror arranged in such a way that the beamsplitter is at a focal plane (see Figure 2.1). The advantage behind this geometry is the small beamsplitter size. Besides being less expensive, this facilitates automatic changing of the beamsplitter, which is convenient in FIR studies where several beamsplitters are often needed to cover the whole spectral range. In the case of the N-O donor IR absorption spectra a single beamsplitter (3.5 μm Mylar) was sufficient for the entire spectral region of interest (about 200-300 cm^{-1}).

A major disadvantage of the Bruker geometry is that a tilt in the moving mirror results in twice the beam misalignment as for a standard Michelson interferometer. With misaligned mirrors the reflected and transmitted beams aren't centered at the same point on the detector and can be shown to give reduced intensity, especially at short wavelengths [86Ga]. Fortunately, the spectral region of the N-O donor IR absorption measurements is not very sensitive to mirror misalignment, and no such problems were encountered in this study.

Both the detector and sample were cooled in a variable temperature liquid He cryostat coupled to the interferometer by a polypropylene window. The light was detected using a Ge bolometer mounted on an

Figure 2.1 IR Absorption Experimental Setup

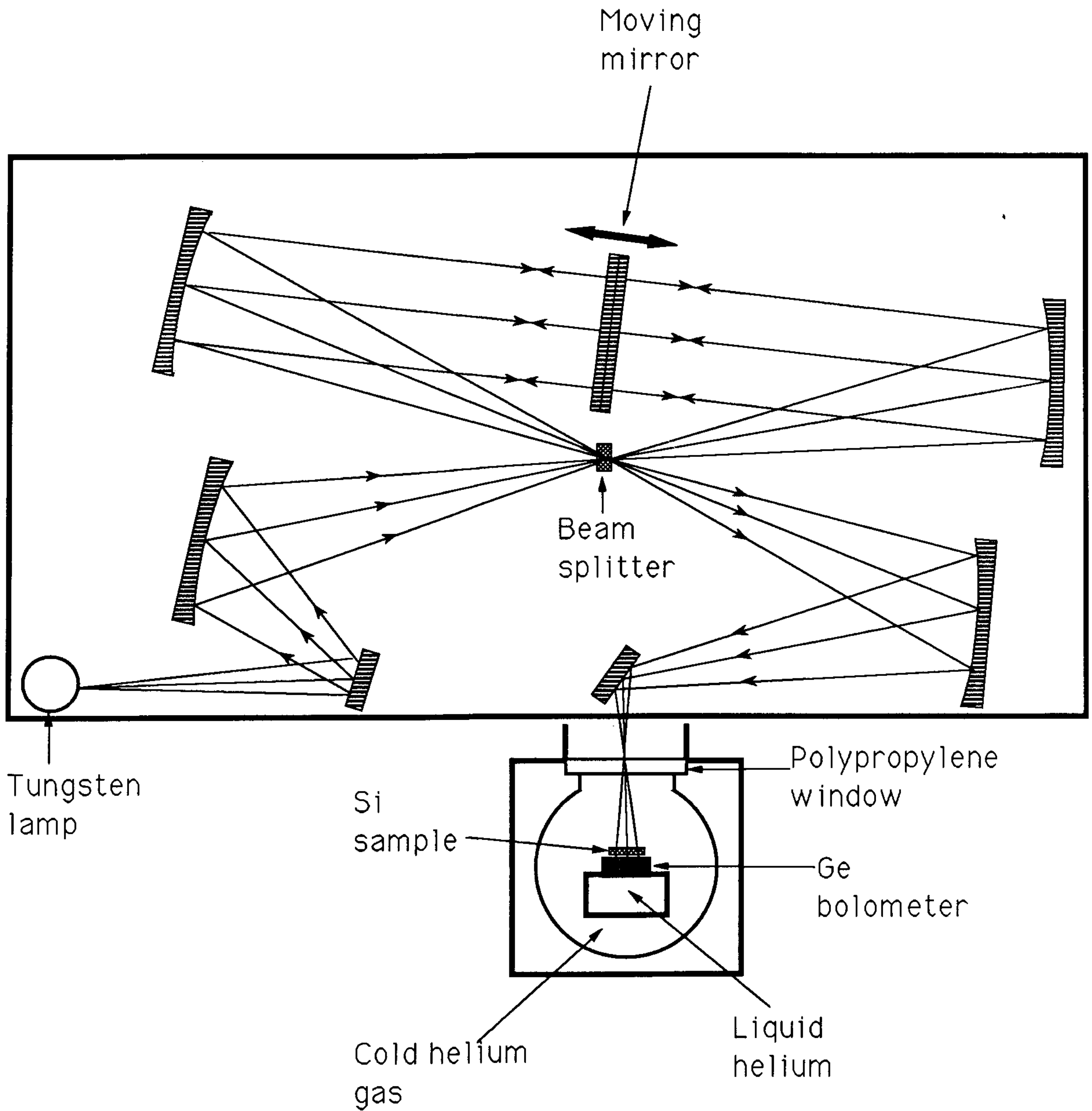

extension from a reservoir of superfluid He. The sample was cooled to 10 K by cold He gas. A calibrated Si diode mounted close to the sample was used to monitor temperature. The IR light source consisted of a tungsten filament lamp. Although a globar source is more intense in the mid IR region, the tungsten lamp provided additional above bandgap light, which by generating electron-hole pairs ensured that impurities were not ionized.

Each spectrum was normalized to that of an untreated float zone (FZ) Si sample of the same thickness, collected under identical experimental conditions. This normalization procedure eliminated features in the spectra due purely to intrinsic Si absorption.

2.2 Photoluminescence Spectroscopy

The basic elements of a PL set-up include a cryogenic system to cool the sample, an excitation source, and a means of detecting the PL at a particular energy. A brief overview of the system used in collecting the data reported in this thesis is given below. A block diagram is shown in Figure 2.2. Considerably more detail can be found in other theses [86Sb, 88S].

Because exciton binding energies are typically less than 10 meV, the sample temperature must be kept low enough that the thermal energy is insufficient to cause dissociation. The samples were cooled to 4.2 K using liquid He in a Janis immersion dewar. When necessary the temperature was further lowered to as little as 1.8 K by pumping the

Figure 2.2 PL Experimental Setup

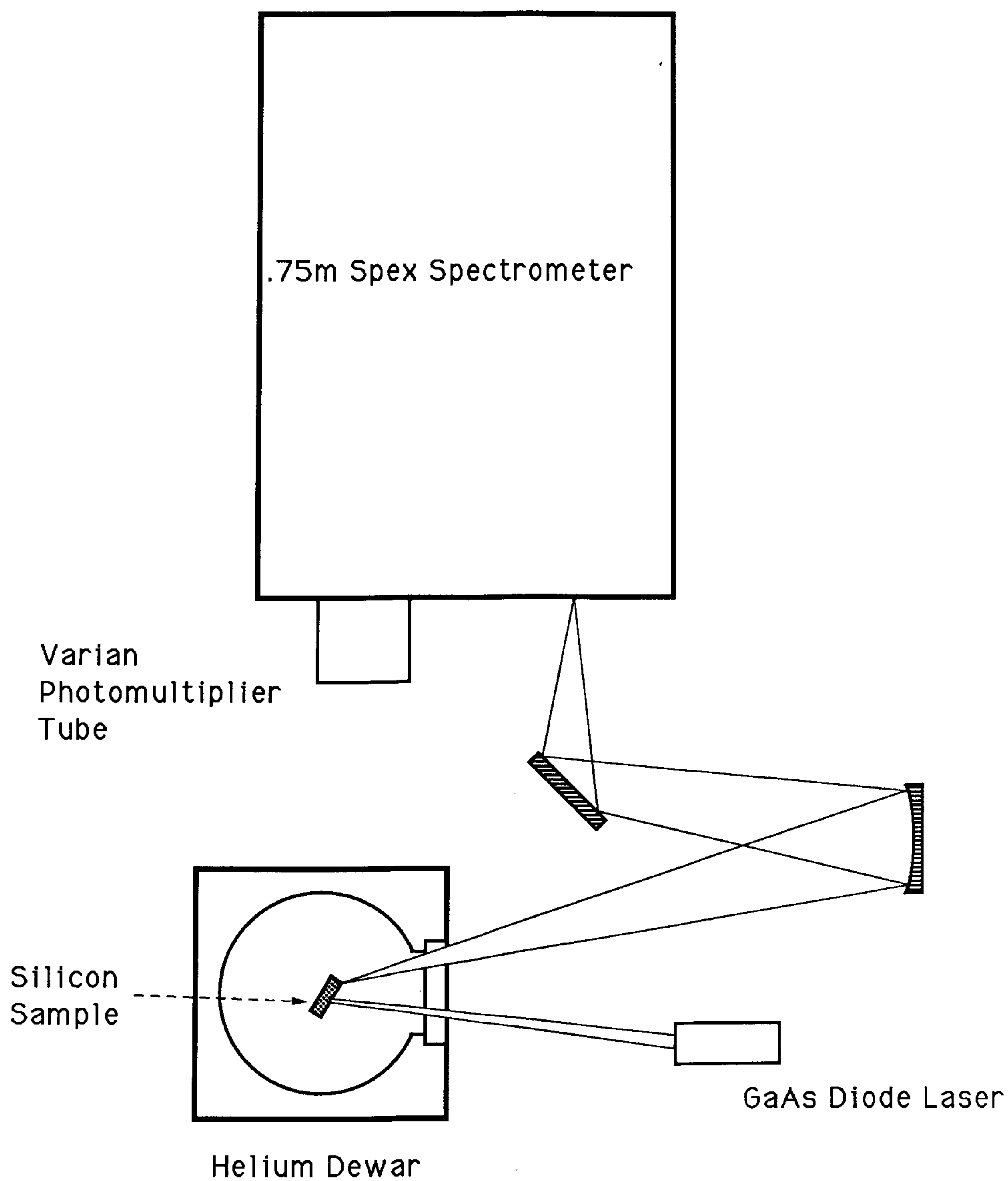

sample chamber. Measurements taken at temperatures below the He lambda point (2.2 K) have the added benefit of a reduction in the noise caused by light scattering in the bubbling He. The temperatures below the lambda point were determined by measuring the vapour pressure above the He liquid.

To create excitons a supply of free carriers is generated by illuminating the sample with light having energy greater than the Si bandgap. Lasers are used since they offer greater intensity than incoherent sources. Suitable excitation sources for Si include the 514.5 nm line of an Ar^+ ion laser or the 676.4 nm line of a Kr^+ ion laser. However, visible light is absorbed within only about 1 μm of the sample surface, so that often these sources result in too large an exciton density, favouring formation of EHDs over BEs and BMECs. With longer wavelength light the absorption coefficient is decreased, therefore resulting in improved bulk excitation. In these experiments a 200 mW GaAs diode laser which emits at about 800 nm was used.

The luminescence was collected by a concave mirror and focused onto the entrance slit of a 0.75 m Spex double spectrometer. The spectrometer was calibrated using the 1.128740 μm Hg emission line from the fluorescent room lights. Resolution for slit widths of 200 μm was 0.41 meV, determined by the FWHM of the Hg line.

The dispersed PL signal was detected using a Varian VPM159A photomultiplier tube. This tube can detect photons with wavelengths ranging from 400 to about 1200 nm and therefore is suitable for most Si no-phonon and phonon replica PL. The detector was cooled to -100°C to reduce the dark count. Because of the high gain and quantum efficiency of this photomultiplier tube, single photons can produce output pulses

large enough to be counted individually. Using this capability of photon counting, signal to noise can be improved over techniques which simply integrate the signal intensity over many pulses, even when lock-in methods are applied. This is because, by setting upper and lower limits on the pulse height acceptable for a single photon count, pulses caused by noise can be rejected. In addition variations in pulse height due to small differences in gain have no effect on photon counts.

2.3 Sample Preparation

Samples suitable for both IR absorption and PL measurements were prepared from oxygen-rich Czochralski (Cz) Si. The oxygen concentration was about 8.8×10^{17} cm^{-3}, as determined from the room temperature absorption by the oxygen local vibration mode at 1106 cm^{-1} [80Ta]. The ratios of BE to FE peak intensities in the TO region indicated contamination of about 4×10^{12} cm^{-3} boron and 2×10^{13} cm^{-3} phosphorus, using the calibration curves of McL Colley and Lightowlers [87M]. Since some oxygen contamination is inherent in Cz grown Si, oxygen-free control samples were prepared from float zone (FZ) Si supplied by Amorphous Materials.

Samples measuring approximately 12 x 6 x 2 mm were cut from the untreated material on a diamond saw. After etching in 10:1 $HF:HNO_3$ to remove saw damage, and cleaning in acetone and then ethanol, the samples were given various thermal treatments. Each sample was treated using a two-step annealing process consisting of a 1 h preanneal at 1270°C,

followed by further annealing for 1 h at a temperature between 550°C and 750°C. After each of these heat treatment stages, the samples were immediately quenched into liquid nitrogen. This was done to prevent the out-diffusion of the N-O donors found by Hara *et al.* to occur during a slow ramp down in temperature [89Hb]. The anneal atmosphere was varied by flowing either oxygen or nitrogen gas through the quartz tube which held the samples.

After the appropriate thermal treatment the samples were simply cleaned in acetone and ethanol then mounted for PL and IR absorption measurements using teflon tape. Although an oxynitride or oxide layer formed on the Si surface during these treatments, removing this layer by polishing with 1 μm diamond paste had no noticeable effect on the PL measurements. The oxynitride did produce a broad band in the IR absorption spectra at about 1000 cm^{-1}, however this did not interfere with the N-O donors since they absorb at energies less than 300 cm^{-1}.

CHAPTER 3 NITROGEN-OXYGEN DONORS IN SILICON

3.1 Introduction

Light element impurities, such as nitrogen, oxygen and carbon, while electrically inactive in Si in their isolated state, can act as shallow donors when grouped together in complexes. The most extensively studied example are the oxygen-related thermal donors, first discovered more than thirty years ago [54F, 57F]. Since then others, including the so-called new donors [81T], "F" series [86V], "S" series [81N], Li-O complexes [81R] and radiation-induced C-O complexes [86D], have been investigated. As with the thermal donors, all these defects can be linked to the presence of oxygen.

Oxygen doping levels in excess of $10^{17}cm^{-3}$ are unintentionally produced in Cz grown Si as a result of containing the molten Si in a silicon dioxide crucible. Annealing the Cz Si near 450°C creates at least nine different oxygen clusters, the thermal donors, all of which behave as double donors whose excited states are described well by effective mass theory [83P, 83O]. Other donors are created by the presence of additional impurities and/or different thermal treatments. Recently several groups [88S, 89Hb, 89Ga] have drawn attention to a series of shallow effective mass-like single donors which are related to the presence of both nitrogen and oxygen in annealed Si. Since nitrogen is often used as an inert gas during device processing or as a reactant in dielectric growth, studies to determine the nature of these defects are especially relevant to device production.

Suezawa *et al.* [86Sc, 88S] studied the IR absorption of oxygen-rich Cz Si which had been deliberately doped with nitrogen by adding Si_3N_4 to the melt. They observed the $1s \Rightarrow 2p_0$ and $1s \Rightarrow 2p_{\pm}$ transitions for five different shallow donors, which they labelled N-O-1 through N-O-5 respectively. Also, the $1s \Rightarrow 3p_0$ transition could be resolved from overlapping phosphorus lines for donors N-O-3 and N-O-4. Because the five lines showed identical separations for the different transitions they were able to dismiss the possibility that several lines might actually originate from stress splitting of a single center. Ionization energies for the donors ranged from 35.38 meV to 37.38 meV as determined by adding the theoretical position of the $2p_{\pm}$ level below the conduction band to the experimental $1s \Rightarrow 2p_{\pm}$ transition energy.

Since relative intensities of different donors in the absorption spectra were found to vary with nitrogen concentration, Suezawa *et al.* [86Sc] suggested that some centers must contain more than one nitrogen atom. This idea was supported by their model of growth kinetics at 479°C completed for donors N-O-3, and a new donor N-O-6 [88S]. This new donor appeared only in samples subjected to a 60 min 1200°C preanneal used to remove all N-O complexes in the as-grown crystal before further anneal treatment. For N-O-3 and N-O-6, the IR absorption was found to saturate at identical levels, although different anneal times were required to reach saturation. The saturation level varied with oxygen, but not nitrogen concentration. The remaining four N-O donors were not considered in the growth model since the absorption data lacked sufficient intensity. Starting with chemical equations of assumed identical reaction constants which build up the complexes in steps assumed to be nitrogen pairs, Suezawa *et al.* [88S] reduce these for

small anneal time (t) to $[A_n] \propto t^{n-1}$, where n represents the number of nitrogen pairs in the complex A_n. Fitting the experimental data resulted in 2 and 3 nitrogen pairs for N-O-6 and N-O-3 respectively.

Hara *et al.* [89Ha, 89Hb] were able to produce the same series of N-O complexes in undoped Cz Si given a high temperature (1270°C) preanneal in a nitrogen atmosphere, followed by a rapid quench to room temperature. Complexes were not observed if the furnace was slowly ramped down in temperature from 1270°C. This was explained by spreading resistance profiles, which when compared to those for quenched samples, seemed to show outdiffusion of the donors from the crystal surface. They also found that while a further anneal at 1000°C annihilated the complexes, one between 600°C and 700°C increased their concentration .

Fitting the spreading resistance profile for a quenched sample annealed at 1270°C for 25 min and 635°C for 90 min to the diffusion equation, a nitrogen diffusion coefficient of 2×10^{-6} cm^2/s was obtained [89Ha]. This value was noted to be five orders of magnitude larger than previously reported values.

Hara *et al.* also completed a study using electron spin resonance data to show that the N-O complexes have C_{2v} symmetry, but were unable to observe any hyperfine interaction with nitrogen [89Hb]. Suggesting an analogy to the thermal donors, they put forward the idea that the ground state of the N-O complexes might also be made up of only a pair of conduction band valleys along the [100] direction.

The direct involvement of nitrogen in these shallow donors has been questioned by Griffin *et al.* [89Ga, 89Gb] This group had previously used photothermal ionization spectroscopy (PTIS) to study the centers and independently observed transitions from seven separate donors in

nominally nitrogen-free Si annealed at 450°C [86Gb, 86N]. Weak lines corresponding to 1s ⇒ $2p_{\pm}$ transitions for three of the donors were also observed in their IR absorption data [86N]. They referred to these defects as the shallow thermal donors (STDs).

Further studies seemed to show that moderate nitrogen doping ([N] ≅ 1.4×10^{15} cm^{-3}) in the Si melt enhanced STD growth, while a higher nitrogen concentration ([N] ≅ 9×10^{15} cm^{-3}) actually decreased it [89Ga, 89Gb]. Also, an unusually low concentration of the oxygen-related thermal donors was observed in all samples doped with nitrogen. Griffin *et al.* proposed that nitrogen acted as a catalyst favouring oxygen agglomerates in the form of STDs instead of the thermal donors. Adding too much nitrogen actually resulted in inhibited diffusion of oxygen and therefore the growth of neither complex. However, these studies did not seem to address the possible role of oxygen concentration in STD growth.

3.2 Infrared Absorption Results

As discussed in Section 2.3, oxygen-rich Cz Si and oxygen-free FZ Si were treated using a two step annealing process consisting of a 1h preanneal at 1270°C, followed by further annealing for 1h at a temperature between 550 and 750°C. When oxygen was used as the ambient gas during the preannealing, no evidence for the generation of the N-O donors was found in the IR absorption spectra for either Cz of FZ Si. By preannealing in nitrogen, however, it was possible to produce the donors in the Cz material (as discussed below), but not in the

oxygen-free FZ Si. These results are in agreement with the findings of Hara *et al.* and suggest that both nitrogen and oxygen are involved in the donor formation [89Hb].

Figure 3.1 illustrates the IR absorption spectra of the N-O donors in two N_2-preannealed Si samples given a further 650°C (Figure 3.1(a)) and 750°C (Figure 3.1(b)) anneal, respectively. The IR absorption measurements were taken using the Bruker interferometer system described in Section 2.1. The five N-O donors are identified in Figure 3.1 beside the $1s \Rightarrow 2p_{\pm}$ transitions according to Suezawa's labelling scheme. For all five N-O complexes $1s \Rightarrow 2p_o$, $1s \Rightarrow 2p_{\pm}$, and $1s \Rightarrow 3p_{\pm}$ transitions were observed. Donors N-O-3 and N-O-5 showed stronger absorption than the other three donors, so that $1s \Rightarrow 3p_o$, $1s \Rightarrow 4p_{\pm}$, and $1s \Rightarrow 5p_{\pm}$ transitions were also seen experimentally. Absorption was not observed for the N-O-6 complex seen by Suezawa *et al.* [88S], or the STD-A complex seen by Griffin *et al.* [89Gb]. Energies for observed N-O donor infrared absorption lines are summarized in Table 3.1.

Although N-O donors were seen in samples given the 1270°C preanneal only, the anneals between 550°C and 750°C increased the intensity of transitions attributed to the N-O donors. The highest concentration of the donors occurred in the 650°C sample, which had 71% absorption through a thickness of 2.2 mm at the $1s \Rightarrow 2p_{\pm}$ transition of N-O-5, giving an absorption coefficient of 5.6 cm^{-1}. Therefore, N-O donors are present in concentrations readily detectable using standard IR absorption techniques.

Ionization energies from the ground state and excited states are shown for each donor in Table 3.2. These values were calculated by using the experimental IR absorption transition energies, and assuming

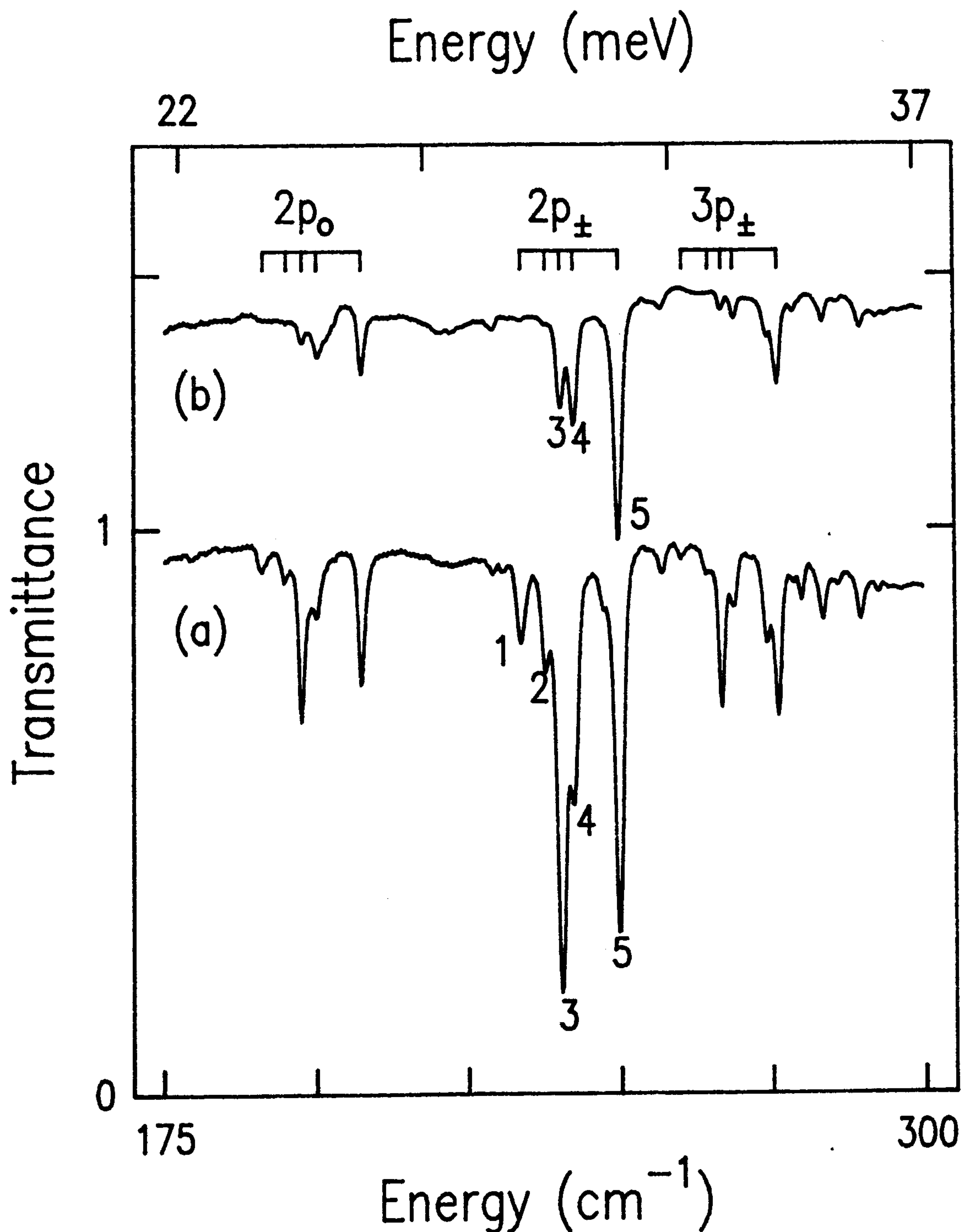

Figure 3.1: Infrared absorption at 10 K from five different nitrogen-oxygen donors in N_2 preannealed Si samples further annealed at (a) 650°C and (b) 750°C. Displayed on the same transmittance scale, with (b) shifted up for clarity. The resolution is 0.5 cm^{-1}.

Table 3.1: N-O Donor IR Absorption Lines

	N-O-1	N-O-2	N-O-3	N-O-4	N-O-5
$1s \Rightarrow 2p_o$	23.70	24.18	24.51	24.80	25.70
$1s \Rightarrow 2p_{\pm}$	28.99	29.50	29.80	30.06	30.99
$1s \Rightarrow 3p_o$		30.69			31.83
$1s \Rightarrow 3p_{\pm}$	32.27	32.82	33.08	33.32	34.25
$1s \Rightarrow 4p_{\pm}$		34.04			35.15
$1s \Rightarrow 5p_{\pm}$		34.73			35.92

Energies of observed N-O donor IR absorption lines in meV. N-O-1 to N-O-5 labelling according to Suezawa's scheme [86Sc]. Transitions were determined by comparing observed energy separations with those of EMT.

Table 3.2 : N-O Donor Ionization Energies

	N-O-1	N-O-2	N-O-3	N-O-4	N-O-5	EMT
$2p_o$	11.69	11.76	11.69	11.64	11.67	11.492
$2p_\pm$	6.41	6.44	6.40	6.38	6.38	6.402
$3p_o$			5.51		5.54	5.485
$4p_\pm$			2.16		2.22	2.187
$5p_\pm$			1.47		1.45	1.449
E_i	35.39	35.94	36.20	36.44	37.37	31.262

Excited state and ground state (E_i) ionization energies in meV for the five N-O donors. Calculated by using the experimental IR absorption transition energies, and assuming the EMT estimate [84J] for the $3p_\pm$ level below the conduction band (3.120 meV). Compared with EMT values taken from Janzén *et al.* [84J].

the EMT estimate of Janzén *et al.* [84J] for the $3p_{\pm}$ level below the conduction band (3.120 meV). Since the $3p_{\pm}$ wave function has zero amplitude at the donor site, this level should show a very small central cell correction. The EMT estimate for the $3p_{\pm}$ level is therefore expected to be very accurate. Ground state ionization energies ranged from 35.39 meV to 37.37 meV, while EMT predicts 31.262 [84J]. Energy levels for the N-O donors are found to be quite well described by EMT, exhibiting only a small central cell correction.

IR absorption data was also collected for energies associated with known local vibrational modes of nitrogen and oxygen. Unfortunately absorption coefficients for nitrogen vibrational modes are small and substitutional nitrogen diffusion in Si is relatively slow [85Sa]. We did not observe the 767 cm^{-1} and 963 cm^{-1} absorption bands reported as local modes of N_2 molecules [86Sa], or the 653 cm^{-1} band due to substitutional N [85S]. Since new vibrational modes which might be attributed to the N-O complexes themselves were also not observed, the absence of the N_2 and substitutional N bands cannot be conclusively attributed to nitrogen being directly incorporated into the N-O complexes. Absorption at 830 cm^{-1} and 1106 cm^{-1}, associated with oxygen-vacancy and interstitial oxygen respectively, could not be distinguished in the untreated Cz Si and N-O complex samples. This may indicate that very little oxygen is actually incorporated in the N-O complexes.

3.3 Photoluminescence Results

The optical phonon assisted PL spectra shown in Figure 3.2 were collected at 1.8 K from the as-received Cz Si boule (Figure 3.2(a)) and from the same 650°C sample discussed in Section 3.2 (Figure 3.2(b)). The experimental set-up was as described in Section 2.2, with the GaAs diode laser used to excite the sample. The LO and TO phonon-assisted free exciton recombination peaks are labelled in the untreated Cz Si spectrum (Figure 3.2(a)) by FE_{LO} and FE_{TO}, respectively. The unresolved weak luminescence from BEs, in the LO region, is indicated by BE_{LO}. The remaining peaks in this spectrum are the TO replicas from BE and BMECs localized at residual boron (B^1 to B^4) or phosphorus (α^1 to α^5, and β^3) [82T]. The superscript in this labelling notation indicates the number of electron-hole pairs present in the initial state. For a complete description of these well known BMECs see the review by Thewalt [82T].

The spectrum from the annealed sample, shown in Figure 3.2(b), contains additional lines not present in the untreated sample. These transitions are from initial exciton states localized on the N-O centers. The most intense transition, which is labelled N-O BE + B^1 in the figure, is the superposition of principal BE lines for excitons bound to the N-O donors, with a further contribution from the boron BE. The large increase in intensity of this line relative to the FE_{TO} intensity in the annealed sample as compared to the $B^1_{TO}:FE_{TO}$ ratio in the untreated material indicates the presence of the N-O complexes in addition to boron. The peak of the strongest line in the TO replica occurs at 1092.85 ±0.05 meV, which is shifted by 0.29 meV to higher energy than the B^1_{TO} transition at 1092.56 meV.

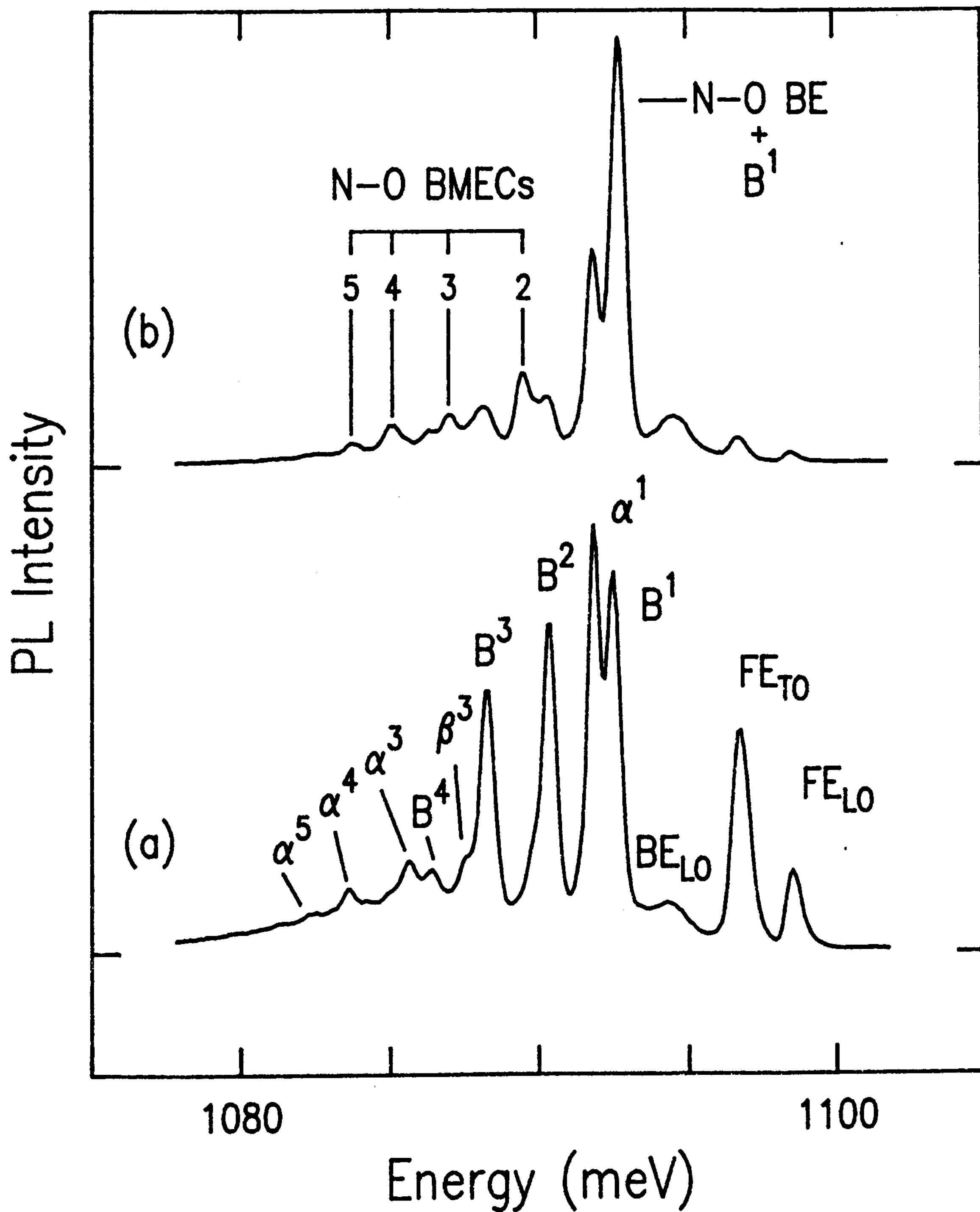

Figure 3.2: Optical phonon-assisted 1.8 K photoluminescence spectra of (a) untreated Si and (b) N_2 preannealed Si further annealed at 650°C.

From Haynes' Rule [60H] the exciton binding energy is predicted to be about a tenth of the impurity ionization energy. The N-O donor ionization energies determined from the IR absorption spectra range from 35.39 meV to 37.37 meV (Table 3.1), so that the 5 different N-O BE lines are estimated to be degenerate to within only 0.2 meV. Therefore the principal luminescence transitions for excitons bound to different donors in the N-O series cannot be resolved in the phonon replica transitions due to phonon lifetime broadening. Unfortunately the no-phonon transitions were not strong enough to be observed. Subtracting the energy of the FE_{TO} edge (1096.7 meV) from the N-O BE + B^1 TO replica, the deduced value for the N-O exciton binding energy is 3.9 meV. The average donor ionization energy is about 9.3 times the observed exciton binding energy and therefore the complexes seem to obey Haynes' rule fairly well. This small discrepancy could be easily accounted for by an apparent shift to lower energy in the N-O BE peak due to overlap with the B^1 BE.

The four other new lines, labelled N-O BMECs 2 to 5 in Figure 3.2, are transitions from initial BMEC states localized on the N-O centers. With increasing excitation power N-O BE, BMEC 2 and BMEC 4 intensities are found to increase exponentially, leveling off due to saturation at very high powers (Figure 3.3). The N-O BE intensity shown in this figure was calculated from the N-O+B^1 peak by assuming the ratio of B^1 to the α^1 line (phosphorus) is the same as in the untreated material. BMECs 3 and 5 were not included since their intensities were found to be too low to get an accurate power dependence. Fitting the low power data the N-O BE, BMEC 2 and BMEC 4 intensities varied as 0.7, 0.9, and 1.3 respectively of excitation power. Although the typical linear and

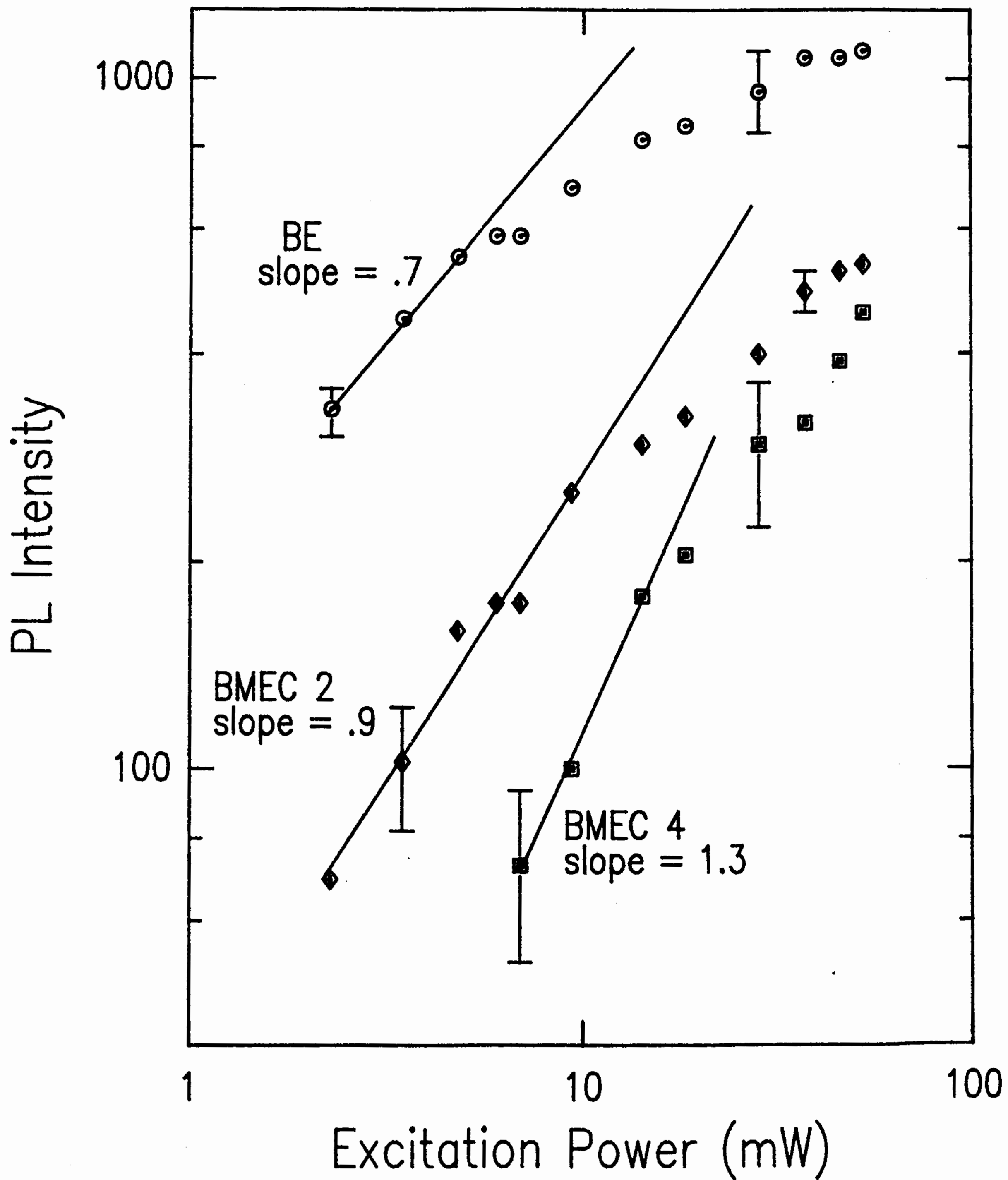

Figure 3.3: Excitation power dependence at 1.8 K of the N-O donor PL intensity in the TO region. N-O BE, BMEC 2 and BMEC 4 PL intensities vary as the powers .7, .9, and 1.3 respectively of excitation power.

superlinear power dependence expected for the BE and BMECs respectively is not observed, there is an obvious increase in power dependence in comparing the BE to BMEC 2 and BMEC 4. The slightly low values for the exponents may result from competing effects due to the presence of boron and phosphorus.

The shell model for BMECs can sometimes be used to infer the nature of the center which binds the excitons [77Kb]. In Figure 3.2(b) the relative intensities of the N-O BMEC lines labelled 3 and 4 are equal, while line 5 is considerably weaker than line 4. This is consistent with a binding center which is a donor, since the closure of the first hole shell (4 holes) occurs with 4 bound excitons, rather than 3 as it would for an acceptor.

The association of the BE with the N-O donors has thus far been based simply on the observation that the luminescence lines are present only in spectra of samples which also exhibit absorption due to the N-O donors. Direct evidence for this association, however, comes from the excited states observed in the 2 *e* region of the PL spectrum. As discussed in Section 1.5, the 2 *e* spectra arise when the BE recombines and leaves the neutral donor in an excited state. Different N-O species can be resolved by their 2 *e* replicas since the N-O donor ionization energies differ by several meV.

In Figure 3.4 spectra in the TO-replica 2 *e* region are shown for (a) the untreated Cz Si, as well as N_2 preannealed samples further annealed at (b) 650°C and (c) 750°C. In the untreated sample, only known phosphorus [76S] and boron [77Tb] transitions are observed. Several new sharp lines appear in the spectra of the treated samples, which can be attributed to 2 *e* replicas of the N-O donors. Energies of

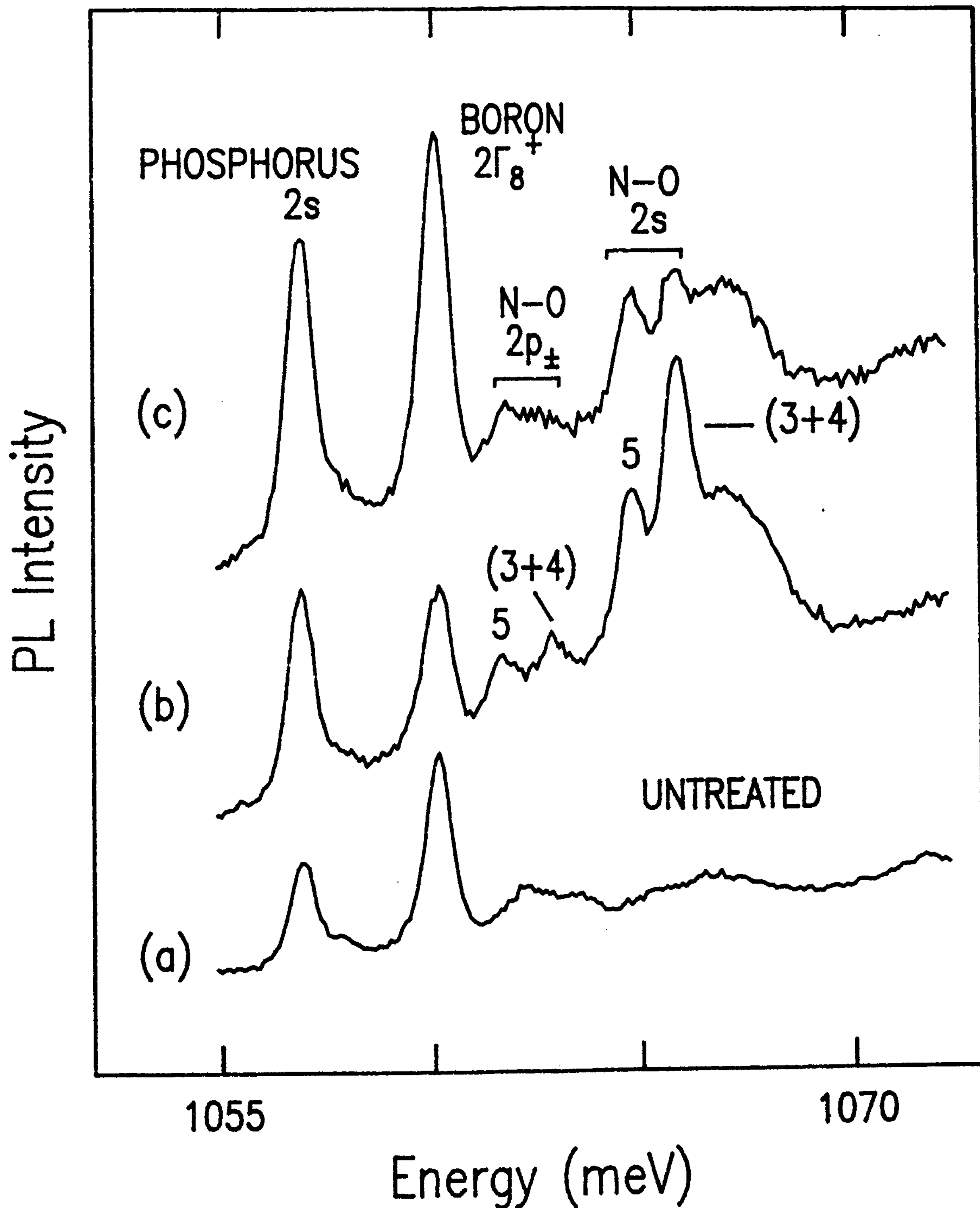

Figure 3.4: Photoluminescence spectra in the bound exciton two electron replica region. Boron and phosphorus excited states are seen in the untreated material (a). Transitions of N-O donors appear in N_2 preannealed Si further annealed at (b) 650°C and (c) 750°C.

all the observed N-O donor PL lines are tabulated in Table 3.3.

The strongest features in the IR absorption spectra of Figure 3.1 are due to the N-O-3, N-O-4, and N-O-5 donors. The expected 0.27 meV splitting of the N-O-3 and N-O-4 transitions is smaller than the resolution in PL, however, and therefore only two features separated by 1.06 meV and related to the unresolved N-O-(3+4) pair and the N-O-5 donor are expected in luminescence. The two strongest new lines in the 2 *e* spectra are separated by 1.1 ±0.2 meV, and therefore correspond to these donor species. This identification is supported by the sample dependence of the intensity ratio of the peaks. The greater intensity of the N-O-(3+4) line in the 650°C sample (Figure 3.4(b)) than in the 750°C sample (Figure 3.4(c)) correlates with the observed behavior for the IR transitions shown in Figure 3.1.

From the discussion in Section 1.4, the strongest 2 *e* replica for a given BE transition should be the one which leaves the donor in its 2s state. From the observed 2 *e* luminescence peaks, the values deduced for the 1s ⇒ 2s transitions are 26.85 ± 0.15 meV for N-O-(3+4), and 27.95 ± 0.15 meV for N-O-5. These give 2s binding energies of 9.47 ± 0.15 meV and 9.42 ± 0.15 meV, respectively, which are only slightly deeper than the effective mass 2s binding energy of 8.856 meV [84J]. These small shifts are consistent with the small positive central cell potentials of the N-O donors observed in the ground state ionization energy values (Table 3.1).

The two smaller sharp peaks seen in Figure 3.4 (b) and (c) are separated from the N-O BE_{TO} line by 29.95 ± 0.15 meV and 31.15 ± 0.15 meV, which agree to within experimental error with the IR 1s ⇒ $2p_{\pm}$ transition energies for the N-O-(3+4) and N-O-5 donors,

Table 3.3 N-O Donor Photoluminescence Lines

N-O PL line (TO Replica)	Energy (meV)
N-O+B BE(1s)	1092.75±.05
N-O BMEC 2	1089.49
N-O BMEC 3	1087.10
N-O BMEC 4	1085.10
N-O BMEC 5	1083.77
N-O-(3+4) BE(2s)	1065.90±.10
N-O-(3+4) BE($2p_{\pm}$)	1062.80
N-O-5 BE(2s)	1064.80±.10
N-O-5 BE($2p_{\pm}$)	1061.60

Observed N-O donor photoluminescence transitions (see Figures 3.2 and 3.4), expressed in meV. In the principal BE line, N-O+B $BE(1s)_{TO}$, contributions from each of the five N-O donors as well as that from boron cannot be resolved. 2*e* satellites were observed for N-O-(3+4), and N-O-5, where the transition labelled N-O-(3+4) consists of unresolved N-O-3 and N-O-4 components.

respectively. The observation of BE transitions to these odd parity N-O donor excited states indicates a relaxation of the usual parity selection rule, perhaps due to the reduced symmetry of these centers [89Ha]. It should also be noted that the broad luminescence band detected on the high energy side of the resolved 2s transitions is located at the energy of the 2 *e* transitions which leave the N-O-(3+4+5) donors in $2p_0$ states, although it is unlikely that this is the only component of this luminescence band.

3.3 Conclusion

BEs and BMECs localized on the N-O donors were observed for the first time using PL spectroscopy. The exciton localization energy was found to be 3.9 meV. From the two electron bound exciton transitions, 2s binding energies of the N-O-(3+4) and N-O-5 donors of 9.47 ± 0.15 meV and 9.42 ± 0.15 meV, respectively, were obtained. The agreement of the excited state energies obtained from PL and IR measurements provides conclusive evidence that the exciton binding centers observed using PL are the same N-O complexes seen in IR absorption. The results of this chapter were published in Appl. Phys. Lett. [90S].

More sophisticated PL techniques such as transient spectroscopy, Zeeman, or uniaxial stress perturbations cannot be used unless the lines can be more clearly resolved. Unfortunately resolution in phonon replicas is limited by phonon broadening. Such experiments may be possible if the N-O donor concentration can be dramatically increased or

sensitivity in the experimental setup improved such that the N-O donors are observed in the no-phonon region. However, further experiments, for example to determine the kinetics behind the N-O donor formation, can be performed using IR absorption data.

CHAPTER 4 NITROGEN DIFFUSION IN SILICON

4.1 Introduction

Since dielectrics, including silicon nitride (Si_3N_4), play a crucial role in IC processing, one would expect that the behaviour of nitrogen in Si would be reasonably well understood. However, compared to oxide growth, surprisingly little is known. Silicon dioxide is grown to thicknesses in excess of one micron by exposing bare Si to O_2 or steam at temperatures of about 900°C. The growth of so-called thermal nitride, performed by substituting N_2 or ammonia gas for the oxygen, is found to be self-limiting. This means that nitride growth effectively comes to a halt after only about 5 min and results in a film of <100 Å in thickness (for reviews see [88R,86J]). The nitride itself is thought to act as a barrier to nitrogen diffusion, preventing a reaction with the Si substrate. Attempts to determine the diffusion coefficient of nitrogen in Si_3N_4 were found to vary widely, possibly because of large differences in structure of the nitride itself [88B]. In fact there is some debate as to whether the nitrogen diffuses through the nitride film at all. Alternative theories propose that, unlike oxidation, film growth does not occur at the film-silicon interface but is a result of diffusion of Si ions to the nitride surface.

A step towards understanding the growth of thermal nitride is to first determine the diffusion rate of N in crystalline Si. The diffusion coefficient (D) at 1200°C was thought to be as little as $\simeq 10^{-11} cm^2/s$ [68C,75D,88N] until recently when a value five orders of magnitude larger was reported by Itoh and Abe [88I]. The greatest

problem in determining D is that unlike other group V elements such as P, As and Bi which behave as donors, nitrogen is electrically inactive in Si. Studies using electron-paramagnetic-resonance (EPR) [82B] and the bombardment by protons to create the nuclear reaction $^{15}N(p,\alpha)^{12}C$ [75M] both indicated that for N implanted Si less than 10 % of the implanted N is incorporated into substitutional sites. This is not surprising considering the relatively small atomic size for N (0.70 Å) compared to Si (1.17 Å) [75M].

It has been suggested [76P] that the nitrogen is predominantly present as N_2 molecules, possibly in interstitial sites. Local vibrational modes (at 766 cm^{-1} and 963 cm^{-1}) associated with N-N pairs bonded to Si have been observed in infrared absorption spectroscopy for both Si doped with N in the melt, and Si implanted with N [86Sa]. However, in Cz Si some nitrogen is suspected to exist in unknown infrared insensitive configurations [85I]. The N-N pair absorption bands have not been reported for N-diffused Si, probably because the absorption coefficient even at the N solubility limit of 4.5×10^{15} cm^{-3} is only about 0.02 cm^{-1} [85I].

Estimates for D reported in the literature are summarized in Table 4.1. The original value given by Clark *et al.* [68C] was based on the p-n junction depth in p-type Si implanted with N. This method is therefore only sensitive to electrically active nitrogen. Another method [75D], intended to be sensitive to molecular nitrogen, electrically activated the diffused N by bombarding the sample with neon ions. After each treatment the electrically active layer was stripped off so that an estimate of the N content was mapped out layer by layer. Unfortunately this study only included diffusions at temperatures

Table 4.1 Diffusion Coefficient of Nitrogen in Silicon

$D(cm^2/s)$	Technique	Problems	
$0.87 \exp(-3.29/kT)$	p-n junction depth	sensitive to electrically active complexes only	[68C]
$3\times10^{-2}\exp(-2.63/kT)$	electrical activ. by Ne	diffusion temperature 700-800°C	[75D]
$\cong10^{-11}$ at 1275°C 1350°C	$^{15}N(\alpha,n)^{18}F$	calibration of activation probability vs depth	[88N]
$2.7\times10^{3}\exp(-2.8/kT)$	SIMS IR absorption	detect $>3\times10^{14}cm^{-3}$ only	[88I]
2×10^{-6} at 1270°C	sheet resistance of N-O donors	N-O conc. assumed proportional to N	[89Hb]

(kT in units of eV)

between 700°C and 800°C. A somewhat similar technique was based on bombardment by α particles and then mapping the concentration of radioactive ^{18}F created by the reaction $^{15}N(\alpha,n)^{18}F$ [88N]. This technique relied on previous measurements of the activation probability of ^{15}N as a function of depth.

The measurements of Itoh and Abe [88I] differ from those in previous publications by directly detecting the N itself, without requiring electrical or radioactive activation. They used SIMS (secondary ion mass spectrometry) to find outdiffused N concentration profiles of annealed FZ Si which had been doped with N in the melt. SIMS intensity was converted to N concentration by calibrating with N implanted reference samples. As well, the decrease in nitrogen concentration agreed with the decrease in absorption by the 963 cm^{-1} N-N absorption peak. Since SIMS cannot detect concentrations less than 3×10^{14} cm^{-3} [88I], this method is not sensitive enough to map N levels for diffusion into the samples. The fitting of N-O donor sheet resistance profiles [89Hb], described in Section 3.1, agreed with the findings of Itoh and Abe. Implicit in this last method is the assumption that N-O donor density is proportional to nitrogen concentration.

4.2 Diffusion Coefficient Determined by Photoluminescence

In this section the diffusion coefficient is calculated by using PL measurements to find the N-O donor depth concentration profile. Because of the extremely good sensitivity of PL to low impurity concentrations this method has the potential to provide much better data than could be obtained by Hara *et al.* [89Hb] using sheet resistance.

N-O donors were created in the usual way (see Section 2.3) by annealing an oxygen rich Cz Si sample in N_2 at 1270°C for 30 min, followed by 635°C for one hour. It is assumed that N diffusion during the 635°C anneal is negligible. The sample was then cut in half lengthwise, so that the PL signal could be collected along this new sample edge, as shown in Figure 4.1. Another cut at a shallow angle (9.4°) to the top face exposed the sample to a depth of about 4.5 mm. After etching in 10:1 $HF:HNO_3$ to remove saw damage, the sample was mounted with the exposed surface approximately perpendicular to the excitation laser beam.

PL spectra were collected at 1.8 K at different points by moving the sample relative to the the laser beam and PL collection optics. As discussed below, the signal can be assumed to originate only from impurities directly illuminated by the excitation source. Sample depth in each case was calculated from the position of the center of the excitation laser beam on the cut away surface. Relative depths are accurate to within about 0.02 mm. However, these depths might be offset by as much as 0.2 mm from the indicated values because of the error in locating the laser at the start of the cut away surface. PL spectra in the TO region are shown in Figure 4.2 for several sample depths. The

Figure 4.1 Sample Geometry

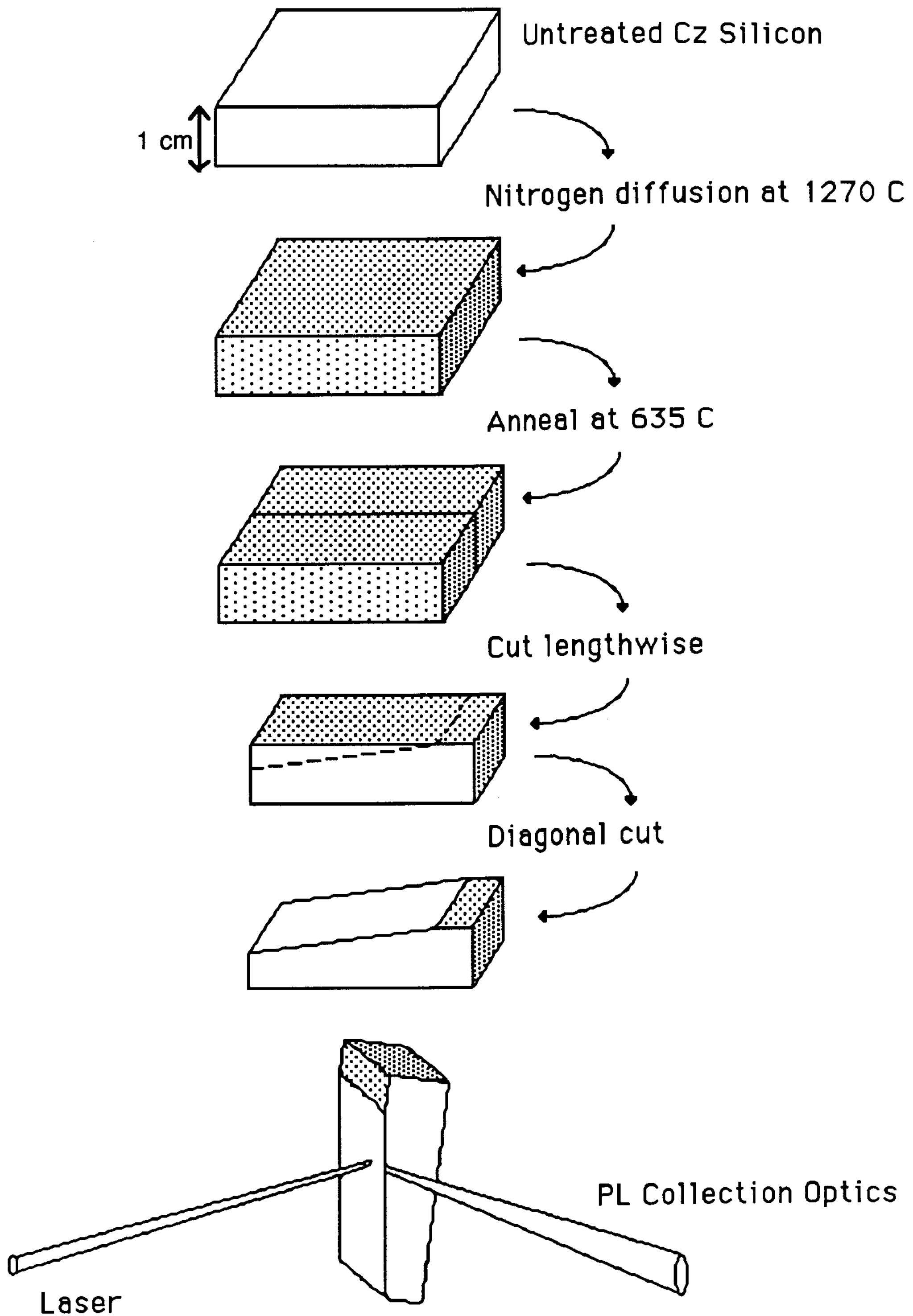

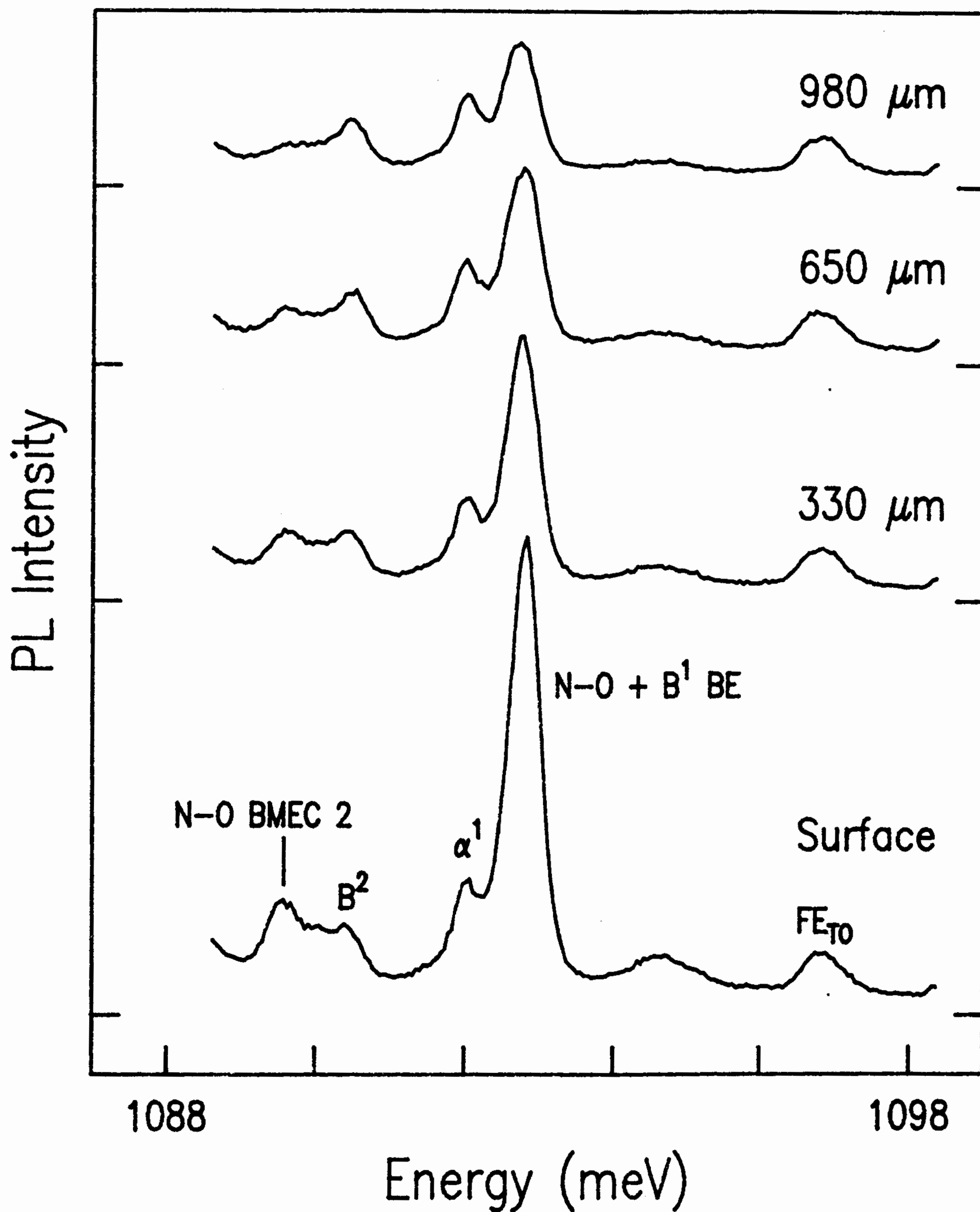

Figure 4.2: N-O donor PL at 1.8 K in the TO region for the sample surface and depths of 330 μm, 650 μm, and 980 μm. Shows the decrease in N-O donor BE and BMEC 2 intensity with increasing sample depth. Normalized to equal FE_{TO} intensity.

N-O+B^1 BE and N-O BMEC 2 intensities are shown to decrease moving away from the surface.

Spatial mapping of impurity concentrations using PL is described by Chen and Lyon [89C], and Tajima *et al.* [80Tb]. The spatial resolution is limited by the diffusion of FEs. Excitons created by the excitation migrate through the Si crystal until they either recombine or are captured by impurities and become bound excitons. In ultrapure Si ($N_A - N_D < 10^{12} cm^{-3}$) Tamor and Wolfe [80Tc] found that the exciton diffusion coefficient was given by $D \cong (300\ cm^2\ K^{1/2}/sec)\ T^{-1/2}$. Assuming a typical free exciton recombination lifetime of $\tau \cong 1\ \mu s$ the diffusion length L, given by $L=(D\ \tau)^{1/2}$, is about 150 μm at 1.8 K. In doped Si the diffusion length is expected to be substantially smaller. Chen and Lyon [89C] reported $L \cong 25\ \mu m$ at 12 K for a sample doped to $10^{16}\ cm^{-3}$, with an even smaller value for L predicted at lower temperatures. Since the sample used in this study is slightly contaminated with boron, phosphorus and the N-O donors themselves, the limit in the concentration mapping resolution due to FE diffusion is conservatively estimated to be 100 μm at 1.8 K.

Several authors describe how to extract quantitatively impurity concentration from PL intensity [78Ta, 80N, 82K, 87M]. At low excitation levels the density of BE is proportional to both the density of FE and of impurities. Therefore the ratio of BE intensity to FE intensity gives an indication of impurity concentration. Because this ratio varies with excitation density, although more so at high excitation levels, it is a good practice to keep the focus and power constant as the laser is stepped across the sample.

NP lines are usually preferred over phonon replicas in determining

impurity concentrations since different impurities are more clearly resolved [87M]. Unfortunately the BE TO replica must be used in this case since the N-O lines cannot be seen in the NP region. This means that contributions due to the unresolved boron BE must be separated from that of the N-O donor BE. A better solution is to use the TO replica of N-O BMEC 2 since it overlaps less with phosphorus and boron lines. Noise caused by the very weak intensity for this peak can be reduced by using integrated peak intensity rather than height.

However, using the BMEC line still hasn't completely eliminated the problem of determining a background. Comparison of the N diffused sample with the untreated material (see Figure 3.2) shows a small shoulder on the boron B^2 line which overlaps with the N-O BMEC 2. Since this shoulder is due to the unresolved phosphorus β^2 BMEC it must be present in the N diffused sample as well. Background due to β^2 can be estimated simply using a spectrum taken deep in the sample where the N-O donor contribution has effectively dropped to zero. A depth of 2.5 mm was assumed to be sufficient since line intensities appeared to have reached a minimum beyond about 2 mm in depth. However, this provides an upper limit on the β^2 background since the nitrogen might actually extend all the way through the sample, so that an approximately constant level near the middle is the minimum. A lower limit for the background due to the β^2 line is obtained simply by assuming it has zero intensity. Figure 4.3 shows the N-O BMEC 2 integrated intensity normalized to FE intensity as a function of sample depth having subtracted off the background in the case of each of the β^2 limits. The theoretical curve (solid line) in this figure is discussed below. Although these profiles differ, especially at low N-O donor concentration, they are shown below

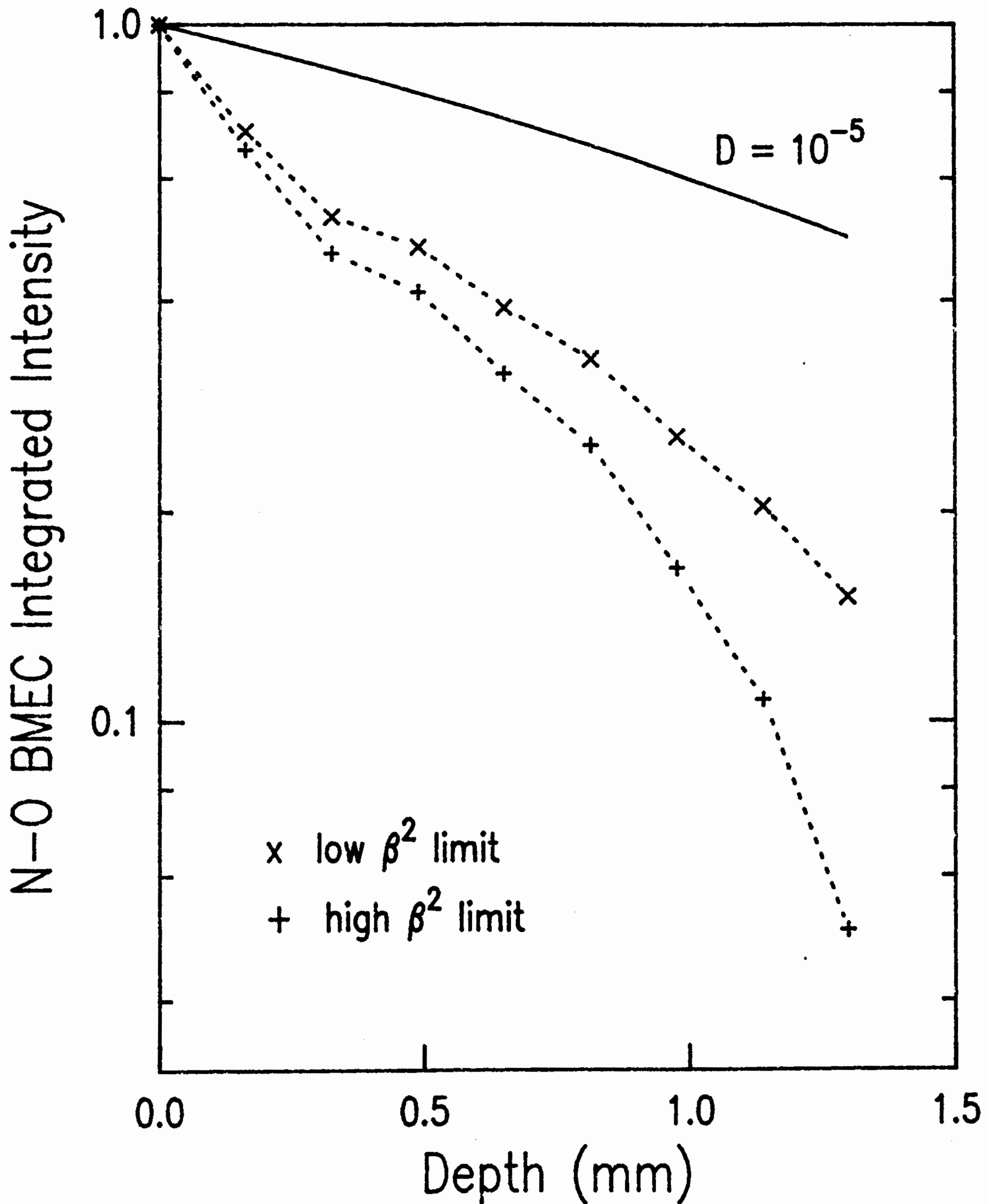

Figure 4.3: N-O BMEC 2 integrated intensity minus β^2 background as a function of sample depth. Normalized to equal FE_{TO} intensity. The two limits for β^2 are discussed in the text. Compared with theoretical profile (see p. 48) for $D = 10^{-5}$ cm^2/sec (solid line).

to lead to only a small difference in the estimated diffusion coefficient.

To calculate the diffusion coefficient from the concentration profile a model describing the diffusion process is needed. As a starting point the diffusion is assumed isotropic, and the diffusion coefficient is taken to be constant. The concentration $C(x,t)$, at a depth x after a diffusion time t, for this simple one-dimensional diffusion is described by solutions to Fick's second law:

$$\frac{\partial C(x,t)}{\partial t} = D\,\frac{\partial^2 C(x,t)}{\partial x^2} \qquad (4.1)$$

under appropriate boundary conditions. The two simplest types of diffusion source, limited supply of diffusion species and constant surface concentration, lead to the Gaussian and complimentary error function solutions respectively:

$$\text{Limited source:} \quad C_l(x,t) = \frac{S}{\sqrt{\pi D t}} \exp\left(-\frac{x^2}{4Dt}\right) \qquad (4.2a)$$

$$\text{Constant source:} \quad C_c(x,t) = C_0 \,\mathrm{erfc}\, \frac{x}{2\sqrt{Dt}} \qquad (4.2b)$$

where S is the total amount of diffusing species initially contained in a single plane at the sample surface, and C_0 is the surface concentration. Since flowing N_2 gas is used for the diffusion, the constant surface concentration equation is probably more appropriate than that of the limited source. However, there is the possibility of a limited diffusion source in the form of the oxynitride layer unavoidably deposited on the sample during the diffusion.

More elaborate solutions than equations 4.2 can be derived (see for

example Crank [75C]) which approximate diffusion from all the sample faces. The PL signal was collected along the new sample edge, about 1.5 cm from the two side faces. Points closer than 0.5 cm to the end faces and bottom face were not included in the data. Therefore N diffusing from the top face will only encounter that coming from other surfaces if significant amounts diffuse further than 0.5 cm. Considering diffusion from one surface only, a concentration at a depth of 0.5 cm of 5% of the surface value requires a diffusion coefficient greater than 10^{-5} cm^2/sec. The resulting profile is shown, assuming a constant concentration source, in Figure 4.3 (solid line). This is compared with the experimental curves of N-O BMEC 2 integrated intensity /FE intensity for the two limits for the β^2 background. Even assuming zero contribution from the β^2 line the theoretical values exceed those actually observed. Similar results are found using the limited diffusion source. Therefore, diffusion of N more than 0.5 cm into the sample is not reasonable and thus the finite sample size can be neglected.

This also implies that the N concentration effectively drops to zero at some depth, so that the upper limit on the background due to β^2 is probably a realistic estimate of the actual β^2 contribution. Figure 4.4 shows the best fit for the constant surface concentration diffusion source, calculated by minimizing numerically the sum of squares of the logarithms of theoretical minus observed concentration. A diffusion coefficient of $1.3 \pm 0.8 \times 10^{-6}$ cm^2/sec was obtained. The upper error for D was estimated by determining the best fit to the profile with the zero β^2 background ($D = 2.1 \times 10^{-6}$ cm^2/sec). For simplicity the same error bar is taken for the lower limit on D. The

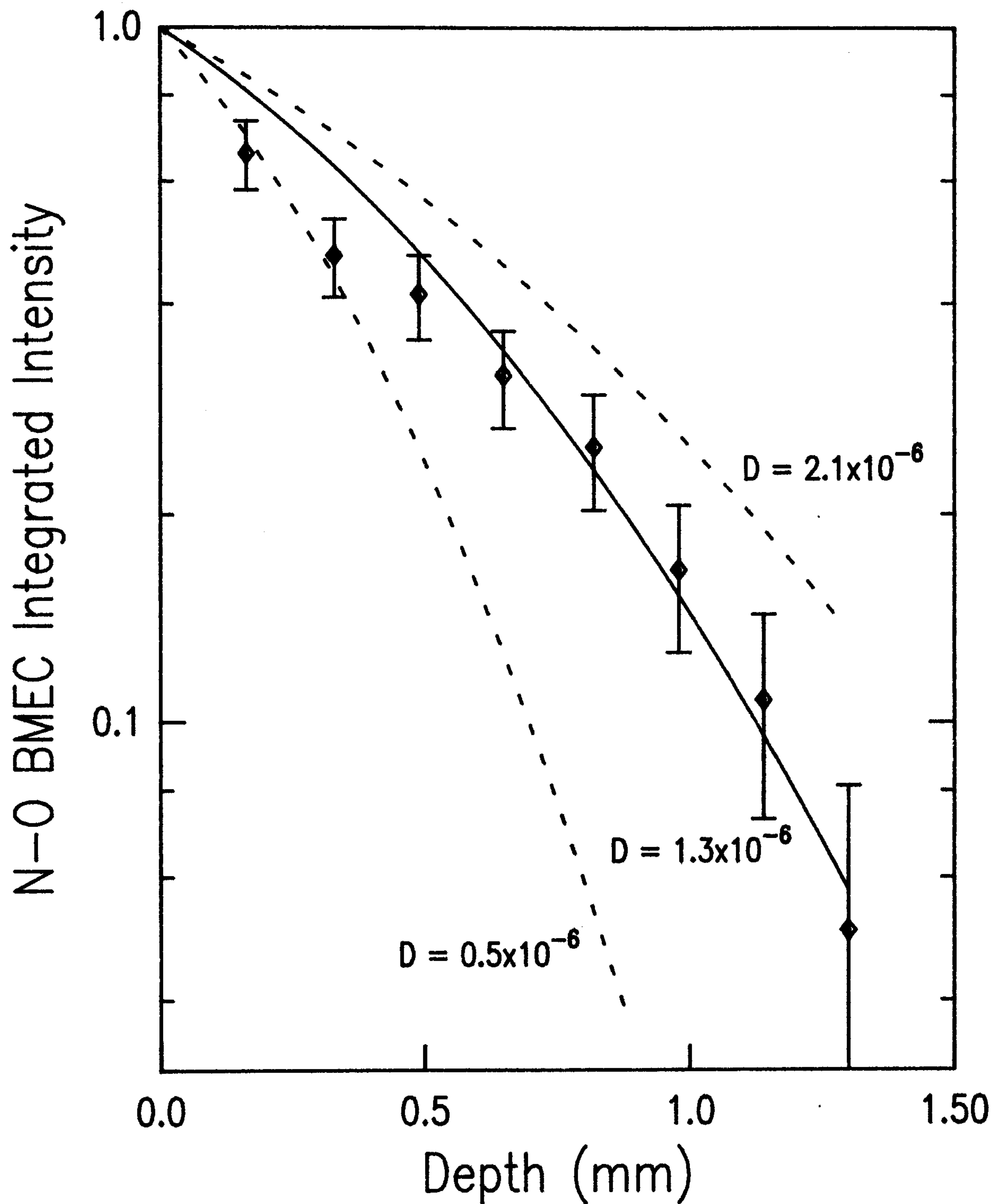

Figure 4.4: N-O BMEC 2 integrated intensity minus β^2 background (upper limit) vs sample depth. Normalized to equal FE_{TO} intensity. Best fit for a constant concentration diffusion source is shown ($D=1.3x10^{-6}$ cm^2/sec), and compared with worst case profiles.

slight kink in the experimental profile at about 0.5 mm in depth is quite interesting, although further measurements are needed to confirm that it is not simply an artifact.

Figure 4.5 shows concentration profiles for the limited diffusion source using diffusion coefficients ranging from 0.5×10^{-6} cm^2/sec to 10^{-6} cm^2/sec. As expected the constant surface concentration source fit the data much better.

4.3 Conclusion

A diffusion coefficient for nitrogen in Si of $1.3 \pm 0.8 \times 10^{-6}$ cm^2/sec was calculated by fitting the N-O donor concentration profile to that predicted by a simple one dimensional diffusion from a constant surface concentration source. Although the precision in the experimental concentration profile could be improved, the sensitivity in the theoretical curve to small changes in D has allowed for a remarkably accurate estimate. This value agrees with the figure 2×10^{-6} cm^2/sec reported by Itoh and Abe [88I] and Hara *et al.* [89b]. There is obvious disagreement with estimates of $D \cong 10^{-11}$ cm^2/sec found in earlier experiments [68C,75D,88N].

Since there was some difficulty in separating the N-O donor PL from that of phosphorus and boron, samples with less contamination would simplify matters greatly. This is unlikely to occur in the near future however, as the Cz Si used in this set of experiments is very good quality by present standards. Another possibility is using different PL

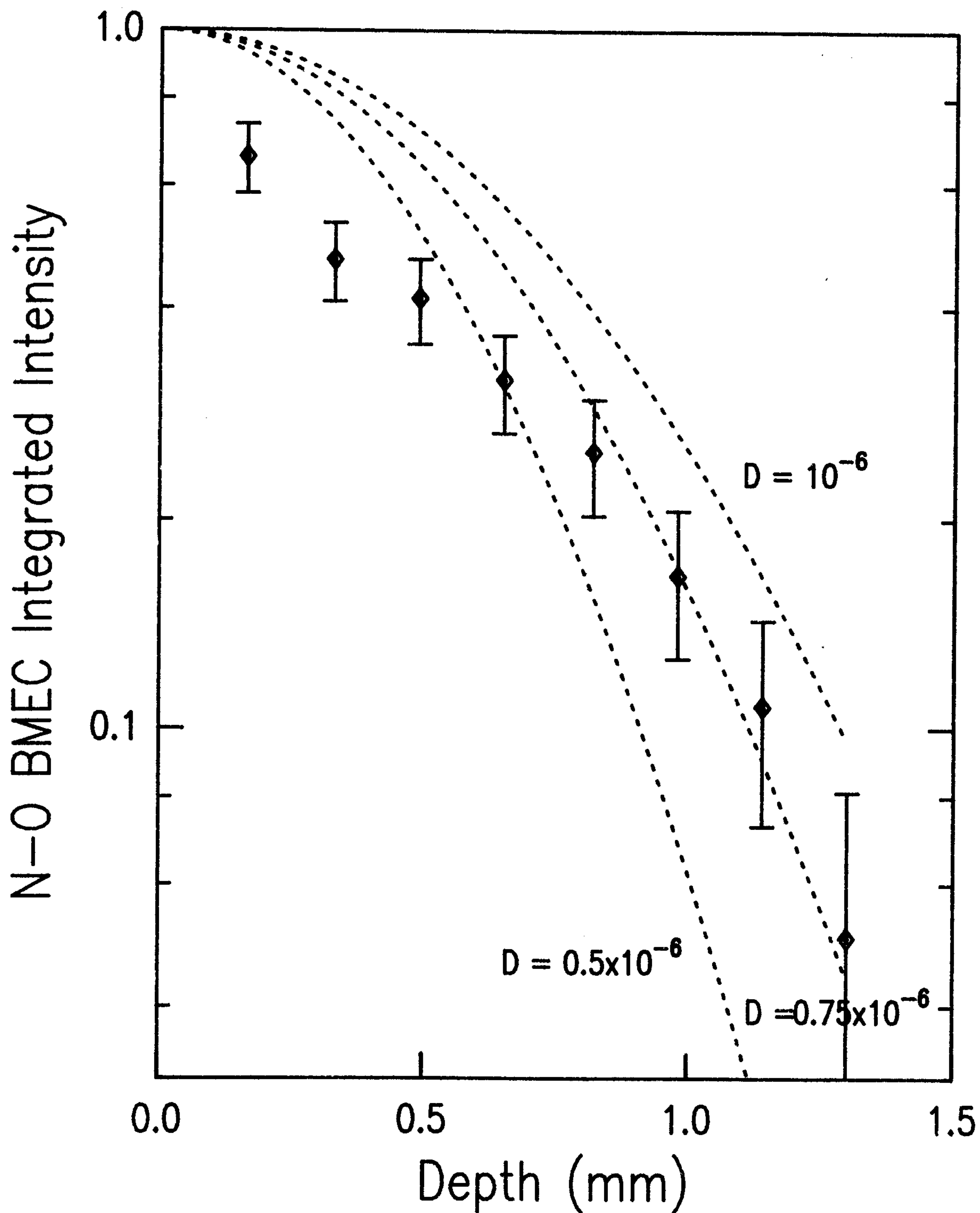

Figure 4.5: N-O BMEC 2 integrated intensity minus β^2 background (upper limit) as a function of sample depth. Normalized to equal FE_{TO} intensity. Theoretical curves for a limited diffusion source with D = 10^{-6}, 0.75×10^{-6}, and 0.5×10^{-6} cm^2/sec shown as dashed lines.

lines such as the 1.1223 eV A,B,C lines also associated with N [84S]. Unfortunately these lines have to date only been observed in samples containing N in excess of $7x10^{14}$ cm^{-3}. Only with more confidence in the concentration profile is it feasible to look at whether the diffusion model should incorporate anisotropic diffusion or a variable diffusion constant.

REFERENCES

54F C.S. Fuller, J.W. Dietzenberger, N.B. Hannay, and E. Buehler, Phys. Rev. **96**, 833 (1954).1954).

57F C.S. Fuller and R.A. Logan, J. Appl. Phys. **28**, 1427 (1957).

55K W. Kohn and J.M. Luttinger, Phys. Rev. **98**, 915 (1955).

58L M.A. Lampert, Phys. Rev. Lett. **1**, 450 (1958).

60H J.R. Haynes, Phys. Rev. Lett. **4**, 361 (1960).

67D P.J. Dean, J.R. Haynes, and W.F. Flood, Phys. Rev. **161**, 711 (1967).

67O A. Onton, P. Fisher, and A.K. Ramdas, Phys. Rev. Lett. **19**, 781 (1967).

68C A.H. Clark, J.D. MacDougall, K.E. Manchester, P.E. Roughan, and F.W. Anderson, Bull. Amer. Phys. Soc. **13**, 376 (1968).

69F R.A. Faulkner, Phys. Rev. **184**, 713 (1969).

70K A.S. Kaminskii and Ya.E. Pokrovskii, Pis'ma Zh ETF **11** , 381 (1970). [Engl. Transl. JETP Lett. **11**, 255 (1970)].

71L N.O Lipari and A. Baldereschi, Phys. Rev. B **3**, 2497 (1971).

73D P.J. Dean, *Luminescence of Crystals, Molecules, and Solutions*, ed. by F.E. Williams (Plenum Press, New York), 538 (1973).1973).

74B A. Baldereschi, and N.O. Lipari, Phys. Rev. B **9**, 1525 (1974).

75B F. Bassani and Pastori Parravicini, *Electronic States and Optical Transitions in Solids* (Oxford Pergamon, 1975).

75D N.V. Denisova, E.I. Zorin, P.V.Pavlov, D.I. Tetelbaum, and A.F. Khokholov, Izv Akad. Nauk SSSR Neorg. Mater. **11**, 2236 (1975).

75M J.B. Mitchell, P.P. Pronko, J. Shewchun, and D.A. Thompson, J. Appl. Phys. **46**, 332 (1975).

76B A. Baldereschi and N.O. Lipari, *Proceedings of Thirteenth International Conference on the Physics of Semiconductors*, Rome, 595 (1976).

76D P.J. Dean, D.C. Herbert, D. Bimberg and W.J. Choyke, Phys. Rev. Lett. **37**, 1635 (1976).

76M T.N. Morgan, *Proceedings of Thirteenth International Conference on the Physics of Semiconductors*, Rome , 825 (1976).

76P P.V. Pavlov, E.I. Zorin, D.I. Tetelbaum, and A.F. Khokhlov, Phys. Stat. Sol. (a) **35**, (1976).

76S R. Sauer, Journal of Luminescence **12/13**, 495 (1976).

77Ha D.C Herbert, P.J Dean, and W.J. Choyke, Solid State Comm. **24**, 383 (1977).

77Hb J.C. Hensel, T.G. Phillips, and G.A. Thomas, Solid State Physics **32**, 88 (1977).

77Ka G. Kirczenow, Solid State Comm. **21**, 713 (1977).

77Kb G. Kirczenow, Can. J. Phys. **55**, 1787 (1977).

77R T.M. Rice, Solid State Physics **32**, 1 (1977).

77Ta M.L.W. Thewalt, Can. J. Phys. **55**, 1463 (1977).

77Tb M.L.W. Thewalt, Solid State Comm. **23**, 733 (1977).

78Ta M. Tajima, Appl. Phys. Lett. **32**, 719 (1978).

78Tb M.L.W. Thewalt, Solid State Comm. **25**, 513 (1978).

79D P.J. Dean and D.C. Herbert, in *Topics in Current Physics* **14**, ed. by K. Cho (Springer, Berlin, Heidelberg, 1979).

80M A.E. Mayer and E.C. Lightowlers, J. Phys. **C12**, L747 (1980).

80N H. Nakayama, T. Nishino, Y. Hamakawa, J. Appl. Phys. **19**, 501 (1980).

80Ta M. Tajima, J. Appl. Phys. **51**, 2247 (1980).

80Tb M. Tajima, A. Yusa, and T. Abe, Jpn. J. Appl. Phys. **19**, suppl 19-1, 631 (1980).

80Tc M.A. Tamor and J.P. Wolfe, Phys. Rev. Lett. **44**, 1703 (1980).

81L M. Lannoo and J. Bourgoin: *Point Defects in Semiconductors I, Theoretical Aspects,* Springer Series in Solid State Sciences, Vol. 35 (Springer, Berlin, Heidelberg, New York, 1981).

81N H. Nakayama, T. Nishino and Y. Hamakawa, Appl. Phys. Lett. **38**, 623 (1981).

81R A.K. Ramdas and S. Rodriguez, Reports on Progress in Physics **44**, 1297 (1981).

81S S.M. Sze: *Physics of Semiconductor Devices* (John Wiley and Sons, 1981).

81T M. Tajima, T. Masui, T. Abe, and T. Iizuka, in *Semiconductor Silicon 1981*, ed.by H.R. Huff, R.J. Kriegler, and Y. Takeishi (Electrochem. Soc., Pennington), 72 (1981).

82B K.L. Brower, Phys. Rev. **B26** , 6040 (1982).

82K A.S. Kaminskii, L.I. Kolesnik, B.M. Leiferou and Ya E. Pokrovskii, J. Appl. Spect. 36, 516 (1982).

82T M.L.W. Thewalt in *Excitons*, ed. by E.I. Rashba and M.D. Sturge (North Holland, New York) 394, (1982).

83O R. Oeder and P. Wagner, in *Defects in Semiconductors II*, ed. by S. Mahajan and J.W. Corbett (North-Holland, New York, 1983).

83P B. Pajot, H. Compain, J. Leroneille, and B. Clerjaud, Physica (Utrecht) **117B**, 110 (1983).

84J E. Janzén, R. Stedman, G. Grossmann, and H.G. Grimmeiss, Phys. Rev. **B29**, 1907 (1984).

85I Y. Itoh, T. Nozaki, T. Masui, and T. Abe, Appl. Phys. Lett. **47**, 488 (1985).

85S H.J. Stein, Appl. Phys. Lett. **47**, 1339, (1985).

86D G. Davies, A.S. Oates, R.C. Newman, R. Woolley, E.C. Lightowlers, M.J. Binns, and J.G. Wilkes, J. Phys. C: Solid State Phys. **19**, 841 (1986).

86Ga P.R Griffiths, and J.A. de Haseth, *Fourier Transform Infrared Spectrometry*, (John Wiley and Sons, 1986).

86Gb J.A. Griffin, H. Navarro, J. Weber, and L. Genzel, in *Proceedings 14th International Conference on Defects in Semiconductors, Paris 1986*, ed. by H.J. Bardeleben , 997, (1986).

86J R.J. Jaccodine, in *Oxygen, Carbon, Hydrogen and .Nitrogen in Crytsalline Silicon*, edited by J.C. Mikkelsen Jr., S.J. Pearton, J.W. Corbett, and S.J. Penneycook (Materials Research Society, Pittsburg 1986), 561 (1986).

86N H. Navarro, J. Griffin, J. Weber, and L. Genzel, Solid State Comm. **58**, 151 (1986).

86Sa H.J Stein, in *Oxygen, Carbon, Hydrogen and Nitrogen in Crytsalline Silicon*, edited by J.C. Mikkelsen Jr., S.J. Pearton, J.W. Corbett, and S.J. Penneycook (Materials Research Society, Pittsburg 1986), 523 (1986).

86Sb T. Steiner, PhD. Thesis, Simon Fraser University (1986).

86Sc M. Suezawa, K. Sumino, H. Harada, and T. Abe, Jpn J. Appl. Phys. 25, L859 (1986).

86V Ph. Vendage, N. Magena and K. Saminadayar, Mat. Res. Soc. **59**, 187 (1986).

87M P. McL Colley and E.C. Lightowlers, Semicond. Sci. Tech. **2**, 157 (1987).

87H E.E. Haller, Mikrochim Acta **III**, 241 (1987).

88B V.I. Belyi, in *Silicon Nitride in Electronics, Materials Science Monographs 34*, 126 (1988).

88C S. Charbonneau, PhD. Thesis, Simon Fraser University (1988).

88I T. Itoh and T. Abe, Appl. Phys. Lett. **53**, 39 (1988).

88N T. Nozaki, Y. Itoh, and Q. Qiu, J. Radioanal. and Nucl. Chem., Articles, **124**, 341, (1988).

88R S.M. Repinsky, in *Silicon Nitride in Electronics, Materials Science Monographs 34*, 19, (1988).1988).

88S M. Suezawa, K. Sumino, H. Harada, and T. Abe, Jpn. J. Appl. Phys. **27**, 62 (1988).

89C Y.H. Chen and S.A. Lyon, IEEE J. Quant. Elect. **25**, 1053, (1989).

89Ga J.A. Griffin, J. Hartung, and J. Weber, Materials Science Forum **38-41**, 619 (1989).

89Gb J.A. Griffin, J. Hartung, J. Weber, H. Navarro, and L. Genzel, Applied Physics **A48**, 41 (1989).

89Ha A. Hara, T. Fukuda, T. Miyabo, and I. Hirai, Jpn. J. Appl. Phys. **28**, 142 (1989).

89Hb A. Hara, T. Fukuda, T. Miyabo, and I. Hirai, Appl. Phys. Lett. **54**, 626 (1989).

90S A.G. Steele, L.C. Lenchyshyn, M.L.W. Thewalt, Appl. Phys. Lett. **56**, 148 (1990).